Exchange and Double-Exchange Phenomena in Linear Homo- and Heterotrinuclear Nickel(II,III,IV) Complexes Containing Six μ_2-Phenolato or μ_2-Thiophenolato Bridging Ligands

Thomas Beissel,[1a] Frank Birkelbach,[1a] Eckhard Bill,[1a] Thorsten Glaser,[1a] Frank Kesting,[1a] Carsten Krebs,[1a] Thomas Weyhermüller,[1a] Karl Wieghardt,*[,1a] Christian Butzlaff,[1b] and Alfred X. Trautwein[1b]

Contribution from the Max-Planck-Institut für Strahlenchemie, D-45470 Mülheim an der Ruhr, Germany, and the Institut für Physik, Medizinische Universität, D-23538 Lübeck, Germany

Received April 22, 1996[⊗]

Abstract: A series of homo- and heterotrinuclear complexes containing three face-sharing octahedra has been synthesized by using the pendent arm macrocyclic ligands 1,4,7-tris(3,5-dimethyl-2-hydroxybenzyl)-1,4,7-triazacyclononane, L^0H_3, and 1,4,7-tris(4-*tert*-butyl-2-mercaptobenzyl)-1,4,7-triazacyclononane, LH_3: $[\{L^0Ni^{II}\}_2Ni^{II}]$ (**1**) and $[\{LCo^{III}\}_2Co^{III}](PF_6)_3$ (**2**); $[\{LCo^{III}\}_2Ni]^{n+}$ ($n = 2$ (**3**), 3 (**4**), 4 (**5**)); $[\{LNi\}_2Co^{III}]^{n+}$ ($n = 1$ (**6**), 2 (**7**), 3 (**8**)) and its linkage isomers $[\{LNi\}Ni\{Co^{III}L\}]^{n+}$ ($n = 1$ (**9**), 2 (**10**), 3 (**11**)) and, finally, the complexes $[\{LNi\}_2Ni]^{n+}$ ($n = 0$ (**12**), 1 (**13**), 2 (**14**), 3 (**15**)). In complex **1** three octahedral Ni^{II} ions form a linear array with two terminal $[L^0Ni^{II}]^-$ moieties in a facial N_3O_3 donor set and a central Ni^{II} ion which is connected to the terminal ions via six phenolate bridging pendent arms of L^0. In complexes **2**−**15** the three metal ions are always in the same ligand matrix yielding an $N_3M(\mu\text{-}S)_3M(\mu\text{-}S)_3MN_3$ first-coordination sphere regardless of the nature of the metal ions (nickel or cobalt) or their formal oxidation states. From temperature dependent magnetic susceptibility measurements it has been determined that **1** has an $S = 3$ ground state whereas in **12** it is $S = 1$. In order to understand this difference in exchange coupling (ferromagnetic in **1** and antiferromagnetic in **12**) in two apparently very similar complexes the magnetic properties of **2**−**15** have been investigated. Complex **3** has an $S = 1$ and **4** an $S = {}^1/_2$, and **5** is diamagnetic ($S = 0$) as is its isoelectronic counterpart **2**. This indicates the availability of the oxidation states II, III, and IV of the central NiS_6 unit. In the isostructural complexes **6**, **7**, and **8**, two terminal nickel ions are bridged by a central diamagnetic Co^{III}. The exchange coupling between two terminal paramagnetic nickel ions was studied as a function of their formal oxidation state. In **6** the two Ni^{II} ions are ferromagnetically coupled ($S = 2$); the mixed-valent $Ni^{II}Ni^{III}$ species **7** has an $S = {}^3/_2$ ground state and in **8** most probably two Ni^{III} ions (d^7 low spin) give rise to an $S = 1$ ground state. In contrast, in the series **9**, **10**, and **11** where two nickel ions are in a position adjacent to each other **9** has an $S = 0$ (antiferromagnetic coupling), but in the mixed-valent complex **10** an $S = {}^3/_2$ ground state (ferromagnetic coupling) is observed. In **11** an $S = 1$ ground state prevails which may be achieved by ferromagnetic coupling between two Ni^{III} ions. For the trinuclear nickel complexes **12**−**15** an $S = 1$ ground state has been determined for **12**, an $S = {}^3/_2$ for the mixed valent complex **13**, and an $S = 2$ for **14**, and **15** exhibits an $S = {}^3/_2$ ground state. The Goodenough−Kanamori rules do not provide a consistent explanation for the observed ground states in all cases. The concept of double exchange, originally introduced by Zener in 1951, appears to provide a more appropriate description for the mixed-valent species **7**, **10**, **13**, **14**, and **15**. This picture is corroborated by the electrochemistry and EPR spectroscopy of complexes.

Introduction

In a classic paper Ginsberg, Martin, and Sherwood[2] reported in 1968 that the linear trimeric cluster $[Ni^{II}_3(acac)_6]$,[3] where acac represents the monoanion pentane-2,4-dionate (acetylacetonate), possesses a septet ground state ($S = 3$). At that time, this was the first example of ferromagnetic exchange interaction in an isolated cluster molecule. Analysis of the temperature dependence of the molar magnetic susceptibility unequivocally demonstrated that intramolecular ferromagnetic exchange coupling between two adjacent octahedral nickel(II) ions (d^8, $S = 1$) and a weaker antiferromagnetic coupling between two terminal Ni^{II} ions prevail. By using the usual isotropic Heisenberg−Dirac−van Vleck (HDvV) exchange Hamiltonian (eq 1) first introduced by Kambe[4] they arrived at numerical values of $+12.5$ cm^{-1} for J_a and -4.5 cm^{-1} for J_t[5]

$$H' = -2J_a[S_1 \cdot S_2 + S_3 \cdot S_2] - 2J_t[S_1 \cdot S_3] \qquad (1)$$

where S_1, S_3 are terminal ion spins and S_2 that of the central metal ion and where J_a represents the coupling constant between adjacent metal ions and J_t that between the terminal metal ions. A zero-field splitting parameter within the septet, D, of -1.3 cm^{-1} and $g = 2.175$ was calculated.

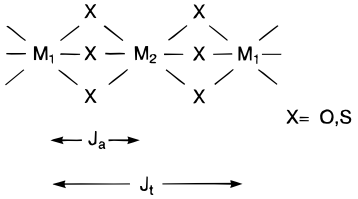

The two exchange pathways were explained in the framework of the Goodenough−Kanamori rules for superexchange:[6] Or-

⊗ Abstract published in *Advance ACS Abstracts,* November 15, 1996.

(1) (a) Max-Planck-Institut für Strahlenchemie, Mülheim an der Ruhr, Germany. (b) Institut für Physik, Medizinische Universität zu Lübeck, Germany.

(2) Ginsberg, A. P.; Martin, R. L.; Sherwood, R. C. *Inorg. Chem.* **1968**, *7*, 932.

(3) Bullen, G. J.; Mason, R.; Pauling, P. *Inorg. Chem.* **1965**, *4*, 456.

(4) Kambe, K. *J. Phys. Chem. Soc. Jpn.* **1950**, *5*, 48.

S0002-7863(96)01305-4 CCC: $12.00

Scheme 1. Ligands

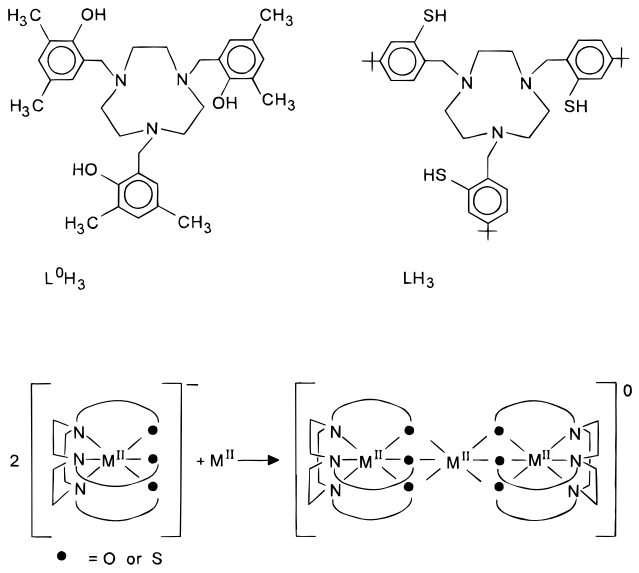

thogonal orbitals of the type $e_g||p_x \perp p_y||e_g$ arising from magnetic metal e_g and filled p orbitals of the bridging oxygens between *adjacent* nickel ions[6] afford ferromagnetic interactions (spin alignment). More difficult to understand is the antiferromagnetic coupling between the terminal nickel ions. The original authors suggested[3,5] that the well-developed π-system of the pentane-2,4-dionato bridging ligand and the half-filled $d_{x^2-y^2}$ orbitals of the terminal nickel ions[5] are correctly orientated to provide an antiparallel spin coupling pathway.

At the beginning of the present investigation we were intrigued by this statement and asked the more general question: to what extent do the sign and magnitude of the exchange coupling between two adjacent and two terminal metal ions in a linear trinuclear complex composed of three face-sharing octahedral entities depend on (i) the nature of the coordinated ligands (with and without "well-developed π-systems") and (ii) the nature of the bridging donor atom? In other words, is the observed coupling in $[Ni_3(acac)_6]$ a special inherent property of this complex or does the geometry (and symmetry) of the $O_3Ni^{II}(\mu\text{-}O)_3Ni^{II}(\mu\text{-}O)_3Ni^{II}O_3$ *core* determine its magnetic properties? Therefore, we have synthesized two complexes containing an $N_3Ni(\mu\text{-}O)_3Ni(\mu\text{-}O)_3NiN_3$ core and its analog $N_3Ni(\mu\text{-}S)_3Ni(\mu\text{-}S)_3NiN_3$ and investigated their magnetism. As two pentane-2,4-dionate anions which chelate the central nickel ion in $[Ni_3(acac)_6]$ simultaneously bridge the pair of terminal nickel ions and thus apparently provide a possible mechanism for antiferromagnetic coupling between the two terminal metal ions, we designed a system which would not provide such a pathway. The pendent arm macrocycles of the type 1,4,7-tris(phenolato)-1,4,7-triazacyclononane are hexadentate ligands which bind strongly to di- and trivalent transition metal ions furnishing thereby an octahedral facial N_3O_3 first coordination sphere around a given metal ion. Since the coordinated three phenolate oxygen atoms are quite basic and orientated *cis* relative to each other, it is often possible to bind a second metal ion at this site and trinuclear complexes containing six μ_2-phenolato bridges can be prepared[7] (Scheme 1). Here we use the ligands 1,4,7-tris(3,5-dimethyl-2-hydroxybenzyl)-1,4,7-triazacyclononane,[8] L^0H_3, and 1,4,7-tris(4-*tert*-butyl-2-mercaptobenzyl)-1,4,7-triazacyclononane,[9,10] LH_3 (Scheme 1), and prepared their trinuclear nickel(II) complexes.

Scheme 2. Synthesized Complexes[a]

$[L^0Ni^{II}Ni^{II}Ni^{II}L^0]^0$	**1**	$[LNi^{II}Co^{III}Ni^{II}L](PF_6)$	**6***
$[LCo^{III}Co^{III}Co^{III}L](PF_6)_3$	**2**	$[LNiCo^{III}NiL](PF_6)_2$	**7**
$[LCo^{III}Ni^{II}Co^{III}L](PF_6)_2$	**3**	$[LNiCo^{III}NiL](PF_6)_3$	**8**
$[LCo^{III}Ni^{III}Co^{III}L]Br_3$	**4**	$[LNi^{II}Ni^{II}Co^{III}L](PF_6)$	**9***
$[LCo^{III}Ni^{IV}Co^{III}L](PF_6)_4$	**5**	$[LNiNiCo^{III}L](PF_6)_2$	**10**
		$[LNiNiCo^{III}L](PF_6)_3$	**11**

$[LNi^{II}Ni^{II}Ni^{II}L]^0$	**12**
$[LNiNiNiL](PF_6)$	**13***
$[LNiNiNiL](PF_6)_2$	**14***
$[LNiNiNiL](PF_6)_3$	**15**

[a] Oxidation numbers are given only in unambiguous cases. The asterisk denotes complexes of which the tetraphenylborate salts were prepared and characterized.

During this study we discovered that the *thio*phenolato bridged species display a rich redox chemistry which its phenolato analog does not. Furthermore, the magnetochemistry of the trinuclear tristhiophenolato complexes proved to be exciting. It has been possible to synthesize a series of 14 homo- and heterotrinuclear complexes. The latter contain one or two paramagnetic nickel in addition to two or more diamagnetic cobalt(III) ion, respectively. The complexes prepared and their labels are given in Scheme 2. Linear homo- and heterotrinuclear, face-sharing octahedral complexes containing six mercapto bridging sulfur atoms are well known[11−20] since their original discovery by Busch and Jicha in 1962[11] and have in a few instances been structurally characterized.[21−23]

As we will show it is possible to isolate a number of mixed-valent $Ni^{II}Ni^{III}$ species. Their electronic structures will be discussed within the concept of double exchange which was originally introduced by Zener[24] in 1951 and revived in recent years.[25] It has been demonstrated to play a role in understanding

(5) Boyd, P. D. W.; Martin, R. L. *J. Chem. Soc., Dalton Trans.* **1979**, 92.
(6) Ginsberg, A. P. *Inorg. Chim. Acta Rev.* **1971**, *5*, 45.
(7) Auerbach, U.; Stockheim, C.; Weyhermüller, T.; Wieghardt, K.; Nuber, B. *Angew. Chem.* **1993**, *105*, 735; *Angew. Chem., Int. Ed. Engl.* **1993**, *32*, 714.
(8) Moore, D. A.; Fanwick, P. E.; Welch, M. J. *Inorg. Chem.* **1989**, *28*, 1504.
(9) Beissel, T.; Bürger, K.-S.; Voigt, G.; Wieghardt, K.; Butzlaff, C.; Trautwein, A. X. *Inorg. Chem.* **1993**, *32*, 124.
(10) Beissel, T.; Glaser, T.; Kesting, F.; Wieghardt, K.; Nuber, B. *Inorg. Chem.* **1996**, *35*, 3936.
(11) Busch, D. H.; Jicha, D. C. *Inorg. Chem.* **1962**, *1*, 884.
(12) Freeh, G.; Chapman, K.; Blinn, E. *Inorg. Nucl. Chem. Lett.* **1973**, *9*, 91.
(13) Brubaker, G. R.; Douglas, B. E. *Inorg. Chem.* **1967**, *6*, 1562.
(14) Blinn, E. L.; Butler, P.; Chapman, K. M.; Harris, S. *Inorg. Chim. Acta* **1977**, *24*, 139.
(15) DeSimone, R. E.; Ontko, T.; Wardman, L.; Blinn, E. L. *Inorg. Chem.* **1975**, *14*, 1313.
(16) Konno, T.; Aizawa, S.; Okamoto, K.; Hidaka, J. *Chem. Lett.* **1985**, 1017.
(17) Johnson, D. W.; Brewer, T. R. *Inorg. Chim. Acta* **1988**, *154*, 221.
(18) Aizawa, S.; Okamoto, K.; Einaga, H.; Hidaka, J. *Bull. Chem. Soc. Jpn.* **1988**, *61*, 1601.
(19) Konno, T.; Aizawa, S.; Hidaka, J. *Bull. Chem. Soc. Jpn.* **1989**, *62*, 585.
(20) Konno, T.; Aizawa, S.; Okamoto, K.; Hidaka, J. *Bull. Chem. Soc. Jpn.* **1990**, *63*, 792.
(21) Heeg, M. J.; Blinn, E. L.; Deutsch, E. *Inorg. Chem.* **1985**, *24*, 1118.
(22) Okamoto, K.; Aizawa, S.; Konno, T.; Einaga, H.; Hidaka, J. *Bull. Chem. Soc. Jpn.* **1986**, *59*, 3859.
(23) Konno, T.; Okamoto, K.; Hidaka, J. *Acta Crystallogr.* **1993**, *C49*, 222.
(24) (a) Zener, C. *Phys. Rev.* **1951**, *81*, 440. (b) Anderson, P. W.; Hasegawa, H. *Phys. Rev.* **1955**, *100*, 675.

the electronic structures of certain Fe_xS_y clusters[26] and the dinuclear mixed-valent complex $[L'Fe^{II}(\mu\text{-}OH)_3Fe^{III}L']^{2+}$.[27]

Experimental Section

The ligands 1,4,7-tris(4-*tert*-butyl-2-mercaptobenzyl)-1,4,7-triazacyclononane trishydrochloride,[9,10] $H_3L\cdot 3HCl$, and 1,4,7-tris(3,5-dimethyl-2-hydroxybenzyl)-1,4,7-triazacyclononane,[8] (L^0H_3), the mononuclear complex [LCo^{III}], and the dinuclear species [LNi^{II}_2Cl][10] have been prepared as described in the literature. The oxidant $[Ni(tacn)_2](ClO_4)_3$[28] and the reductant $[(tmcn)Cr(CO)_3]$[29] (tacn = 1,4,7-triazacyclononane; tmcn = 1,4,7-trimethyl-1,4,7-triazacyclononane) were also prepared according to published procedures.

Preparation of Complexes. $[L^0Ni^{II}Ni^{II}Ni^{II}L^0]$ (1). A methanolic solution (50 mL) of the ligand H_3L^0 (0.265 g; 0.5 mmol) and triethylamine, NEt_3 (0.25 mL), was added to a methanolic solution (50 mL) of $NiCl_2$ (0.10 g; 0.75 mmol) at ambient temperature with stirring. The solution was heated to reflux for 20 min and cooled to 10 °C. A yellow-green precipitate of **1** formed immediately which was collected by filtration. Yield: 0.12 g (40%).

$[LCo^{III}Co^{III}L](PF_6)_3$ (2). A suspension of $CoCl_2\cdot 6H_2O$ (0.05 g; 0.21 mmol) and [LCo^{III}] (0.30 g; 0.42 mmol) in methanol (50 mL) was heated to reflux for 30 min in the presence of air, after which time a clear deep brown solution was obtained. To the filtered solution a saturated methanolic solution (20 mL) of $NaPF_6$ was added which initiated the precipitation of brown microcrystals of **2**. Yield: 0.35 g (86%). 400 MHz ^{1}H NMR spectrum (CD_3CN): δ = 7.53 (H_a; $^3J_{H_aH_b}$ = 8.0 Hz; $^3J_{H_aH_c}$ = 2.0 Hz, 6H); 7.25 (H_b; $^3J_{H_bH_a}$ = 8.0 Hz, 6H); 6.15 (H_c; $^4J_{H_cH_a}$ = 2.0 Hz; 6H); 5.32 (H_d; $^2J_{H_dH_e}$ = 16.0 Hz; 6H); 3.94 (H_e; $^2J_{H_eH_d}$ = 16.0 Hz; 6H); 3.54 (H_f; $^2J_{H_fH_h}$ = 14.0 Hz; $^3J_{H_fH_i}$ = 4.0 Hz); 3.42 (H_g, $^2J_{H_gH_i}$ = 13.0 Hz; $^3J_{H_gH_h}$ = 5.0 Hz; 6H); 3.15 (H_h; $^2J_{H_hH_f}$ = 14.0 Hz; $^3J_{H_hH_g}$ = 5.0 Hz, 6H) 2.78 (H_i; $^2J_{H_iH_g}$ = 13.0 Hz; $^3J_{H_iH_f}$ = 4.0 Hz, 6H), 1.05 (H_j: 54H). See Chart 1 for proton labels.

$[LCo^{III}Ni^{II}Co^{III}L](PF_6)_2$ (3). A suspension of $NiCl_2\cdot 6H_2O$ (0.10 g; 0.42 mmol) and [LCo^{III}] (0.60 g; 0.84 mmol) in methanol (50 mL) was heated under argon to reflux for 30 min until a clear brown solution was obtained. To the filtered solution was added a saturated solution of $NaPF_6$ in methanol (20 mL) whereupon a brown microcrystalline precipitate of **3** formed. Yield: 0.64 g (85%).

$[LCo^{III}Ni^{III}Co^{III}L]Br_3$ (4). To a solution of **3** (0.20 g; 0.12 mmol) in methanol (60 mL) was added one drop of elemental bromine. The color of the solution changed immediately to bluish-brown. After stirring at ambient temperature for 30 min, a dark microcrystalline precipitate formed. Yield: 0.15 g (72%).

Chart 1

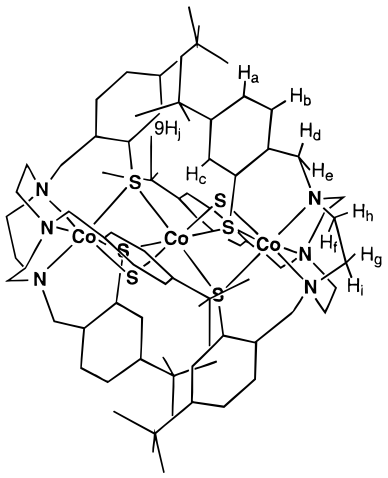

$[LCo^{III}Ni^{IV}Co^{III}L](PF_6)_4$ (5). To a solution of **3** (0.20 g; 0.12 mmol) in methanol (50 mL) were added two drops of methanesulfonic acid and PbO_2 (50 mg). The resulting suspension was stirred at room temperature for 30 min during which time the color changed to deep violet. To the filtered solution was added a solution of $NaPF_6$ (0.20 g) in methanol (30 mL). Upon cooling to 4 °C a black, microcrystalline precipitate formed. Yield: 0.14 g (66%).

$[LNi^{II}Co^{III}Ni^{II}L](PF_6)$ (6). A suspension of 1,4,7-triazacyclononane (64 mg; 0.48 mmol) in degassed methanol (40 mL) and [LNi^{II}_2Cl] (0.20 g; 0.25 mmol) was gently stirred and heated to 50 °C under argon for 20 min. To the cooled (20 °C), clear, light-green solution was added dropwise a methanolic solution (20 mL) of $CoCl_2\cdot 6H_2O$ (30 mg; 0.13 mmol) under an argon atmosphere. The solution was heated to reflux for 60 min and then cooled to 20 °C. Exposure of this solution to air initiated a color change to red-brown. To the filtered solution was added $NaPF_6$ (0.20 g) dissolved in methanol (30 mL). Upon storage at 4 °C, red-brown microcrystals of **6** were obtained. Yield: 0.10 g (49%).

The tetraphenylborate salt, $[L_2Ni_2Co]BPh_4$ (**6***), was obtained from an acetonitrile solution (40 mL) of **6** (0.10 g) by addition of $Na[BPh_4]$ (0.20 g) in CH_3CN (20 mL) and storage of the solution at 4 °C as brown microcrystals. Yield: 0.10 g (90%).

$[LNiCo^{III}NiL](PF_6)_2$ (7). Ferrocenium hexafluorophosphate, $[Fc]PF_6$ (21 mg; 0.06 mmol), was added to a solution of **6** (0.10 g; 0.06 mmol) in methanol (40 mL). After the mixture was stirred for 10 min at ambient temperature a clear solution was obtained to which $NaPF_6$ (0.20 g) dissolved in methanol (20 mL) was added. Upon storage of this solution at 4 °C for a few hours a microcrystalline precipitate of **7** formed. Yield: 0.08 g (73%).

$[LNiCo^{III}NiL](PF_6)_3$ (8). $[Ni(tacn)_2](ClO_4)_3$ (28 mg; 0.045 mmol) was added to a solution of **7** (0.08 g; 0.045 mmol) in acetonitrile (30 mL) whereupon the color of the solution changed to deep-red. After the mixture was stirred for 10 min, $NaPF_6$ (0.20 g) dissolved in CH_3CN (15 mL) was added. The solvent was nearly completely removed by rotary evaporation and the residue was washed with water (50 mL). Yield: 80 mg (92%).

$[LiNi^{II}Ni^{II}Co^{III}L](PF_6)$ (9). Under an argon blanketing atmosphere [LNi_2Cl] (0.17; 0.21 mmol) and [LCo^{III}] (0.15 g; 0.21 mmol) in methanol (30 mL) were heated to reflux for 3 h during which time a brown-black microcrystalline precipitate of [LNiNiCoL]Cl formed which was filtered off, washed with diethyl ether, and air-dried. Yield: 0.25 g (78%). Anal. Calcd for $C_{78}H_{108}N_6S_6Ni_2CoCl$: C, 61.1; H, 7.1; N, 5.5; S, 12.5. Found: C, 60.9; H, 7.4; N, 5.3; S, 12.6.

The corresponding tetraphenylborate salt, $[LNi^{II}Ni^{II}Co^{III}L]BPh_4$ (**9***), was prepared from a solution of **10** (0.25 g; 0.14 mmol) in acetonitrile (30 mL) under argon to which $[(tmcn)Cr(CO)_3]$[29] (tmcn = 1,4,7-trimethyl-1,4,7-triazacyclononane) (43 mg; 0.14 mmol) was added as reductant. The solution was heated to reflux for 30 min. To the cooled (20 °C) solution was added $Na[BPh_4]$ (0.20 g) in CH_3CN (10 mL)

(25) (a) Belinskii, M. I.; Tsukerblat, B. S.; Gerbeleu, N. V. *Sov. Phys. Solid State* **1983**, *25*, 497. (b) Girerd, J.-J. *J. Chem. Phys.* **1983**, *79*, 1766. (c) Borshch, S. A. *Sov. Phys. Solid State* **1984**, *26*, 1142. (d) Noodleman, L.; Baerends, E. J. *J. Am. Chem. Soc.* **1984**, *106*, 2316. (e) Blondin, G.; Girerd, J.-J. *Chem. Rev.* **1990**, *90*, 1359. (f) Blondin, G.; Borshch, S.; Girerd, J.-J. *Comm. Inorg. Chem.* **1992**, *12*, 315.

(26) (a) Papaefthymiou, V.; Girerd, J.-J.; Moura, I.; Moura, J. J. G.; Münck, E. *J. Am. Chem. Soc.* **1987**, *109*, 4703. (b) Noodleman, L. *Inorg. Chem.* **1988**, *27*, 3677. (c) Noodleman, L. *Inorg. Chem.* **1991**, *30*, 256. (d) Borshch, S. A.; Chibotaru, L. F. *Chem. Phys.* **1989**, *135*, 375. (e) Ding, X.-Q.; Bill, E.; Trautwein, A. X.; Winkler, H.; Kostikas, A.; Papaefthymiou, V.; Simopoulos, A.; Beardwood, P.; Gibson, J. F. *J. Chem. Phys.* **1993**, *99*, 6421. (f) Bominaar, E. L.; Hu, Z.; Münck, E.; Girerd, J.-J.; Borshch, S. A. *J. Am. Chem. Soc.* **1995**, *117*, 6976. (g) Bominaar, E. L.; Borshch, S. A.; Girerd, J.-J. *J. Am. Chem. Soc.* **1994**, *116*, 5362. (h) Girerd, J.-J.; Papaefthymiou, V.; Surerus, K. K.; Münck, E. *Pure Appl. Chem.* **1989**, *61*, 805.

(27) (a) Drüeke, S.; Chaudhuri, P.; Pohl, K.; Wieghardt, K.; Ding, X.-Q.; Bill, E.; Sawaryn, A.; Trautwein, A. X.; Winkler, H.; Gurman, S. J. *J. Chem. Soc., Chem. Commun.* **1989**, 59. (b) Ding, X.-Q.; Bominaar, E. L.; Bill, E.; Winkler, H.; Trautwein, A. X.; Drüeke, S.; Chaudhuri, P.; Wieghardt, K. *J. Chem. Phys.* **1990**, *92*, 178. (c) Gamelin, D. R.; Bominaar, E. L.; Kirk, M. L.; Wieghardt, K.; Solomon, E. I. *J. Am. Chem. Soc.* **1996**, *118*, 8085. (d) Gamelin, D. R.; Bominaar, E. L.; Mathoniere, C.; Kirk, M. L.; Wieghardt, K.; Girerd, J.-J.; Solomon, E. I. *Inorg. Chem.* **1996**, *35*, 4323.

(28) (a) Wieghardt, K.; Schmidt, W.; Herrmann, W.; Küppers, H.-J. *Inorg. Chem.* **1983**, *22*, 2953. (b) Wieghardt, K.; Walz, W.; Nuber, B.; Weiss, J.; Ozarowski, A.; Stratemeier, H.; Reinen, D. *Inorg. Chem.* **1986**, *25*, 1650.

(29) Beissel, T.; Della Vedova, B. S. P. C.; Wieghardt, K.; Boese, R. *Inorg. Chem.* **1990**, *29*, 1736.

(30) *International Tables for Crystallography*; Kynoch: Birmingham, England, 1974; Vol. IV, pp 99 and 149.

(31) Miyanowaki, S.; Konno, T.; Okamoto, K.; Hidaka, J. *Bull. Chem. Soc. Jpn.* **1988**, *61*, 2987.

whereupon a dark brown-black precipitate formed. Yield: 99 mg (39%). Anal. Calcd for $C_{102}H_{128}BCoN_6Ni_2S_6$: C, 67.4; H, 7.1; N, 4.6; S, 10.6; Co, 3.2. Found: C, 67.8; H, 7.2; N, 4.4; S, 10.7; Co, 3.1.

The hexafluorophosphate salt, **9**, was prepared as described above by addition of $NaPF_6$ instead of Na[BPh_4].

[LNiNiCo^{III}L](PF$_6$)$_2$ (10). The chloride salt of **9** (0.25 g; 0.16 mmol) was suspended in methanol (50 mL) and [Fc]PF_6 (54 mg; 0.16 mmol) was added. The resulting suspension was heated to reflux for 30 min after which time $NaPF_6$ (0.20 g) dissolved in CH_3OH (15 mL) was added. Cooling to −18 °C for 2 h produced a microcrystalline precipitate of **10**. Yield: 0.16 g (56%).

[LNiNiCo^{III}L](PF$_6$)$_3$ (11). To a solution of **10** (0.10 g; 0.056 mmol) in acetonitrile (30 mL) was added [Ni(tacn)$_2$](ClO_4)$_3$ (35 mg; 0.056 mmol), whereupon the color changed to deep violet. After the mixture was stirred for 20 min at 20 °C $NaPF_6$ (0.20 g) in CH_3CN (15 mL) was added. The solvent was removed by rotary evaporation and the residue was suspended in water (40 mL) and then filtered off. Yield: 95 mg (88%).

[LNi^{II}Ni^{II}Ni^{II}L]^0 (12). A solution of nickel(II) acetate (0.52 g; 2.1 mmol), the ligand H_3L·3HCl (1.0 g; 1.4 mmol), and triethylamine (0.5 mL) in methanol (50 mL) was heated to reflux under an argon blanketing atmosphere for 4 h. During this procedure a microcrystalline brown precipitate formed which was collected by filtration, washed with acetone and diethyl ether, and air-dried. Yield: 0.35 g (33%).

[LNiNiNiL](PF$_6$) (13). A suspension of **12** (0.13 g; 0.87 mmol) and **14** (see below) (0.16 g; 0.87 mmol) in CH_3OH (60 mL) was heated to reflux under argon for 30 min until a clear violet solution was obtained. Upon cooling of the solution to 4 °C a violet precipitate formed. Yield: 0.24 g (91%).

The corresponding tetraphenylborate salt, [LNiNiNiL]BPh_4 (**13***), was obtained from an acetonitrile solution (50 mL) of **13** (0.10 g) to which a solution of Na[BPh_4] (0.20 g) in CH_3CN (15 mL) was added. Storage at 4 °C for 2 h produced deep-violet microcrystals. Anal. Calcd for $C_{102}H_{128}BN_6Ni_3S_6$: C, 67.4; H, 7.1; N, 4.6; S, 10.6. Found: C, 68.0; H, 7.1; N, 4.9; S, 10.1.

[LNiNiNiL](PF$_6$)$_2$ (14). [Fc]PF_6 (89 mg; 0.27 mmol) was added to a suspension of **12** (0.20 g; 0.13 mmol) in methanol (50 mL). The reaction mixture was stirred at 50 °C for 30 min until a deep blue, clear solution was obtained. Addition of a solution of $NaPF_6$ (0.20 g) in CH_3OH (15 mL) and cooling to 4 °C initiated the precipitation of black-blue microcrystals of **14**. Yield: 0.20 g (86%).

The corresponding tetraphenylborate salt, [LNiNiNiL](BPh_4)$_2$ (**14***), was obtained from an acetonitrile solution (50 mL) of **14** (0.20 g) to which a solution of Na[BPh_4] (0.20 g) in CH_3CN (15 mL) was added. Storage at 4 °C for 2 h produced black-blue microcrystals. Anal. Calcd for $C_{126}H_{148}B_2N_6Ni_3S_6$: C, 70.8; H, 7.0; N, 3.9; S, 9.0. Found: C, 70.2; H, 6.8; N, 3.9; S, 9.1.

[LNiNiNiL](PF$_6$)$_3$ (15). To a solution of **14** (0.25 g; 0.13 mmol) in acetonitrile (30 mL) was added [Ni(tacn)$_2$](ClO_4)$_3$ (0.10 g; 0.16 mmol). The solution was stirred at 20 °C for 30 min during which time the color changed to grayish-blue. Addition of a saturated solution of $NaPF_6$ in CH_3CN (15 mL) and reduction of the reaction volume by rotary evaporation of the solvent and cooling to 4 °C produced a microcrystalline precipitate which was filtered off, washed with water and diethyl ether, and air-dried. Yield: 0.20 g (80%).

All complexes gave satisfactory elemental analyses; the data are available in the supporting information.

Physical Measurements. The magnetization of powdered samples of complexes were measured in the temperature range 2 to 295 K on a SQUID magnetometer (MPMS, Quantum Design) in a magnetic field of 1.0 T. For calculation of the molar magnetic susceptibilities, χ_M, the diamagnetism of the sample was taken into account by using tabulated Pascal's constants. Correction for temperature-independent paramagnetism per trinuclear complex was also applied (see Results). The 400-MHz ^{1}H NMR spectra were recorded on a Bruker AM 400 FT spectrometer with the solvent as the internal standard. Continuous wave EPR spectra were measured at temperatures of 2.8−10 K on a Bruker ESP 300e spectrometer equipped with a helium cryostat ESR 910 (Oxford Instruments). Electronic spectra were recorded on a Perkin Elmer Lambda 9 spectrophotometer in the range 200−2000 nm.

X-ray Crystal Structure Determinations. The crystallographic data of [{LNi}$_2$Ni][BPh_4] (**13***) and [{LNi}$_2$Ni](PF_6)$_2$·5acetone (**14**) are summarized in Table 1. A dark brown prismatic crystal of **13*** was placed on a Siemens R3m/V diffractometer and a blue-black crystal of **14** on a Siemens SMART system; graphite monochromated Mo Kα X-radiation was used throughout. Intensity data collected at 295 K for **13*** and at 173 K for **14** were corrected for Lorentz, polarization, and absorption effects (ψ-scans) in the usual manner. The structures were solved by conventional Patterson and difference Fourier methods by using the Siemens SHELXTL-PLUS package (G. M. Sheldrick, Universität Göttingen). The function minimized during full-matrix least-squares refinement was $\sum w(|F_o| - |F_c|)^2$, where $w^{-1} = \sigma^2(F) + 0.0005F^2$. Neutral atom scattering factors and anomalous dispersion corrections for non-hydrogen atoms were taken from ref 30. The hydrogen atoms were placed at calculated positions with isotropic thermal parameters; the methyl groups were treated as rigid bodies. All non-hydrogen atoms were refined with anisotropic thermal parameters.

Table 1. Crystallographic Data for [{LNi}$_2$Ni]BPh_4 (**13***) and [{LNi}$_2$Ni](PF_6)$_2$·5acetone (**14**)

formula	$C_{102}H_{128}BN_6Ni_3S_6$	$C_{93}H_{138}F_{12}N_6Ni_3O_5P_2S_6$
fw	1817.4	2078.5
cryst syst	monoclinic	monoclinic
space group	*C*2/*c*	$P2_1/n$
a (Å)	26.019(5)	15.7962(4)
b (Å)	23.218(5)	13.2130(3)
c (Å)	17.510(4)	23.9344(6)
β (deg)	98.07(3)	92.866(1)
V (Å^3)	10473(4)	4989.2(2)
T (K)	295(2)	173(2)
Z	4	2
ρ_c (g cm^{-3})	1.153	1.383
λ(Mo Kα) (Å)	0.71073	0.71073
μ(Mo Kα) (mm^{-1})	0.694	0.794
cryst dimens (mm)	0.32 × 0.45 × 0.50	0.4 × 0.4 × 0.4
no. of independent reflcns	3226 ($F > 4.0\sigma(F)$)	18514 ($F > 4.0\sigma(F)$)
R_f[a]	0.069	0.0625

[a] $R_F = \sum(|F_o| - |F_c|)/\sum|F_o|$.

Results

Synthesis of Complexes. The preparation and crystal structure of the gray mononuclear species [LCo^{III}] has been recently described[10] as has the synthesis of the dinuclear complex [LNi^{II}Ni^{II}Cl]. In this latter complex one nickel(II) ion is in an octahedral *fac*-N_3S_3 donor environment whereas the second Ni(II) ion is tetrahedrally bound to three bridging thiolate sulfur atoms and one terminal chloride ligand (S_3Cl-donor set). The structure type is face-sharing octahedral/tetrahedral. Both complexes are used as starting materials for the preparation of the present series of complexes. We have successfully employed the following mononuclear complexes as effective one-electron oxidants: ferrocenium hexafluorophosphate, [Fc]PF_6, bis(1,4,7-triazacyclononane)nickel(III) triperchlorate,[28] [Ni^{III}(tacn)$_2$](ClO_4)$_3$; and [(1,4,7-trimethyl-1,4,7-triazacyclononane)-tricarbonylchromium(0)],[29] [(tmcn)Cr(CO)$_3$], as one-electron reductant. The redox potentials have been determined for the couples [Fc]$^+$/Fc, [Ni(tacn)$_2$]$^{3+/2+}$, and [(tmcn)Cr(CO)$_3$]$^{+/0}$ to be 0.0, 0.55, and −0.57 V *vs* Fc$^+$/Fc, respectively.

Reaction of the ligand 1,4,7-tris(3,5-dimethyl-2-hydroxybenzyl)-1,4,7-triazacyclononane,[8] L^0H_3, and triethylamine with $NiCl_2$ (L^0H_3:Ni = 2:3) in methanol produces a green-yellow precipitate of [L^0Ni^{II}Ni^{II}Ni$^{II}L^0$] (**1**). Crystals of **1** consist of neutral trinuclear molecules composed of three face-sharing octahedra where the two terminal nickel ions are in a *fac*-N_3O_3 donor set of three tertiary amines and three phenolato oxygen atoms, respectively, and the central nickel ion is coordinated to six bridging phenolates (Scheme 1). Similarly, the reaction of [LCo^{III}] with $CoCl_2$·6H_2O (2:1) in methanol generates in the presence of dioxygen a deep brown solution from which upon addition of $NaPF_6$ brown microcrystals of [{LCo^{III}}$_2$Co^{III}](PF_6)$_3$

Scheme 3. Synthetic Routes to Heterotrinuclear Complexes

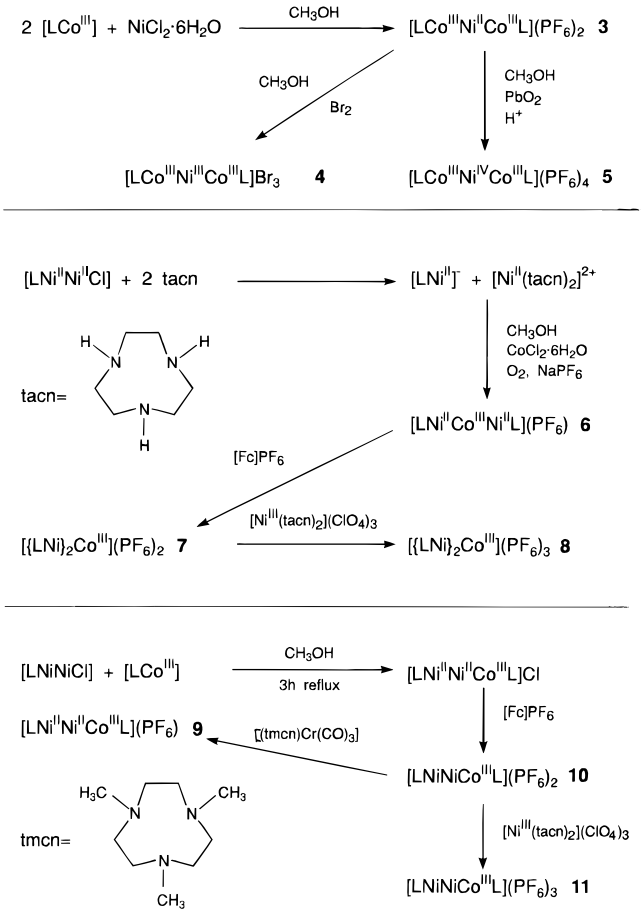

(**2**) are obtained. The coordinated mercapto groups in [LCo^{III}] function as a tridentate donor toward a central Co^{III} ion (CoS_6 octahedron). The 400-MHz ^1H NMR spectrum of **2** in CD_3CN displays 10 proton signals which are assigned as in the Experimental Section and Chart 1. The trication has S_6 symmetry. No indications for dynamic behavior of the methylene groups of 1,4,7-triazacyclononane backbone or of the aromatic pendent arms were detected even at room temperature. The signals are similar to those reported for mononuclear [LIn^{III}].[10]

Replacing $CoCl_2 \cdot 6H_2O$ by $Ni^{II}Cl_2 \cdot 6H_2O$ affords brown crystals of [$\{LCo^{III}\}_2Ni^{II}$]$(PF_6)_2$ (**3**) upon addition of $NaPF_6$ to the reaction mixture (Scheme 3). Similar linear trinuclear complexes [$\{Co^{III}(aet)_3\}_2M]^{n+}$ have been synthesized (M^{II} = Co^{II}, Ni^{II}, $n = 2$; and M^{III} = Co^{III}, $n = 3$) and structurally characterized.[11−23]

Depending on the oxidizing capability of an added oxidant complex **3** can be oxidized by one electron yielding the trication [$\{LCo^{III}\}_2Ni^{III}]^{3+}$ or by two electrons with formation of the tetracation [$\{LCo^{III}\}_2Ni^{IV}]^{4+}$ which are isolable as the hexafluorophosphate salts **4** and **5**, respectively. Complex **4** is formed by oxidation of **3** with Br_2 and **5** is obtained from **3** when PbO_2 in the presence of methanesulfonic acid is used as oxidant (Scheme 3). As we will show these oxidations are metal-centered and genuine Ni^{III} and Ni^{IV} containing trinuclear complexes are thus accessible.

We have demonstrated previously[10] that the reaction of [Ni^{II}-$Ni^{II}Cl$] with 2 equiv of 1,4,7-triazacyclononane (tacn) in methanol produces quantitatively the green mononuclear species [$LNi^{II}]^-$ and violet [$Ni^{II}(tacn)_2]^{2+}$. The monoanion [$LNi^{II}]^-$ is very stable in solution and should also function as a tridentate ligand toward other labile metal ions. That this is indeed the case is demonstrated by the reaction of [LNi]$^-$ with $Co^{II}Cl_2 \cdot 6H_2O$ (2:1) in methanol in the presence of air which affords, upon addition of $NaPF_6$, red-brown crystals of [$\{LNi^{II}\}_2Co^{III}$]-(PF_6) (**6**). Reaction of **6** with 1 equiv of [Fc]PF_6 produces dicationic [$\{LNi\}_2Co^{III}$]$(PF_6)_2$ (**7**). Simple charge considerations assuming the presence of two trianions L^{3-} and one cobalt(III) center immediately imply that the dication in **7** is a mixed-valent $Ni^{II}Ni^{III}$ species. Interestingly, **7** can be further oxidized by using the stronger one-electron oxidant $[Ni^{III}(tacn)_2](ClO_4)_3$ which generates the tricationic complex [$\{LNi\}_2Co^{III}$]$(PF_6)_3$ (**8**) which can be formulated as a species containing two Ni^{III} ions (Scheme 3).

Scheme 4. Synthetic Routes to Homotrinuclear Nickel Complexes

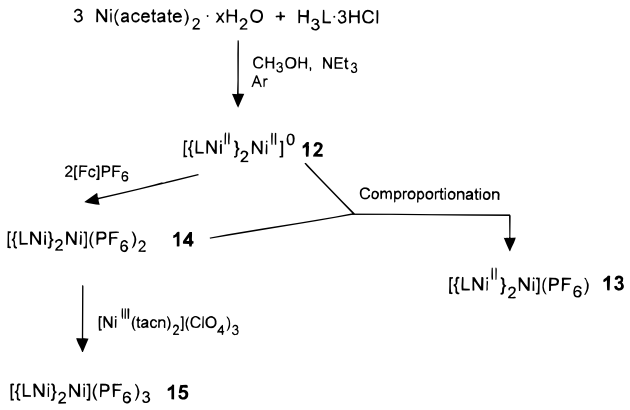

In complexes **6**, **7**, and **8** the nickel ions—irrespective of their actual oxidation state—always occupy the terminal positions in the linear trinuclear face-shearing octahedral assembly of the metal ions and the cobalt ion is in the central position in a CoS_6 environment. The use of mononuclear relatively inert [LNi]$^-$ and of labile $Co(OH_2)_6^{2+}$ in the synthesis necessitates this arrangement provided that scrambling of the metal ions does not occur. The challenge was, of course, to prepare the linkage isomers of **6**, **7**, and **8**, namely complexes [$LNiNiCo^{III}L]^{+/2+/3+}$, where a nickel and a cobalt ion occupy each one of the two terminal positions with an additional nickel ion in the central position. This was achieved by the following procedure (Scheme 3): Reaction of [LNiNiCl] with 1 equiv of [LCo^{III}] in refluxing methanol under anaerobic conditions generates after 1 h a solution which contains three species: the desired [LNi^{II}-$Ni^{II}Co^{III}L]^+$ (violet), [$LNiNiNiL]^+$ (violet), and [$LCo^{III}Ni^{II}$-$Co^{III}L]^{2+}$ (red brown) which can be easily separated by column chromatography (Kieselgel 60; mobile phase 1:1 mixture of diethyl ether and acetone). We then found that refluxing of the above reaction mixture for prolonged time (∼3 h) produces a homogeneous brown-black precipitate of pure [LNiNiCoL]-Cl in 78% yield. This material is insoluble in most common organic solvents and water but it is possible to oxidize this complex with 1 equiv of [Fc]PF_6 in methanol. From the resulting clear solution, upon addition of $NaPF_6$, the dicationic salt [$LNiNiCo^{III}L](PF_6)_2$ (**10**) is obtained as microcrystalline solid. Oxidation of **10** with 1 equiv of $[Ni^{III}(tacn)_2](ClO_4)_3$ yields [$LNiNiCo^{III}L](PF_6)_3$ (**11**) whereas the corresponding monocationic salt [LNiNiCoL](PF_6) (**9**) is generated by reduction of **10** with 1 equiv of [(tmcn)$Cr(CO)_3$].

From the reaction mixture of the uncoordinated ligand, $H_3L \cdot$ 3HCl, and nickel(II) acetate (ratio 2:3) in methanol under anaerobic conditions to which NEt_3 was added, a microcrystalline brown precipitate of [$LNi^{II}Ni^{II}Ni^{II}L]^0$ (**12**) is obtained (Scheme 4). This complex is insoluble in all common organic solvents and water but a suspension of **12** in methanol, to which 2 equiv of [Fc]PF_6 were added, produces a clear deep blue solution from which a blue-black microcrystalline precipitate

Table 2. Electrochemical Data of Complexes[a]

	redox potential $E_{1/2}$, V *vs* Fc^+/Fc				
complex	$4+/3+^b$	$3+/2+^b$	$2+/1+^b$	$1+/0^b$	$0/-1^b$
2		−0.65(r)			
3	+0.52(r)	+0.11(r)			
6	+0.72(qr)	+0.09(r)	−0.32(r)		
9	+0.64(qr)	+0.09(r)	−0.40(r)		
14	+0.71(qr)	+0.24(r)	−0.38(r)	−0.76(r)	
$[LNi^{II}]^-$				−0.29(ir)	−0.68(qr)

[a] Conditions: acetonitrile solution; 0.10 M tetra-*n*-butylammonium hexafluorophosphate supporting electrolyte; ferrocene (~10^{-3} M) as internal reference; 20 °C; glassy carbon working electrode; Ag/AgCl (saturated LiCl in C_2H_5OH) reference electrode; scan rate 100 mV s^{-1}; r = reversible and qr = quasireversible ($E_{1/2} = (E_p^{ox} + E_p^{red})/2$); ir = irreversible $E = E_p^{ox}$. [b] Charge of the complex couple.

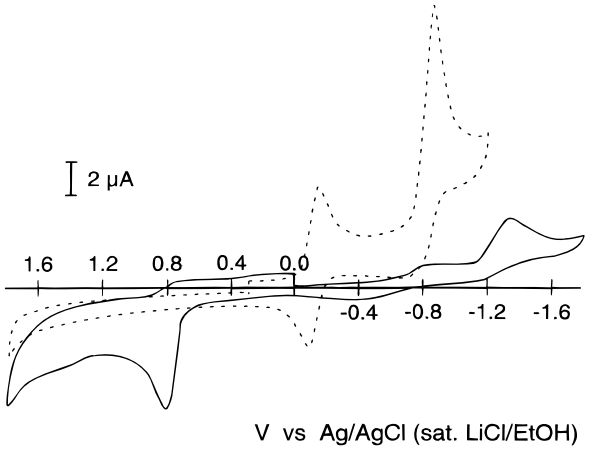

Figure 1. Cyclic voltammogram of $[LCo^{III}]$ (—) and $[L_2Co^{III}_3](PF_6)_3$ (**2**) (···) in CH_3CN (0.10 M $[N(n\text{-}Bu)_4]PF_6$, glassy carbon working electrode, scan rate 100 mV s^{-1}).

of $[L_2Ni_3](PF_6)_2$ (**14**) is obtained in 86% yield. Heating of 1 equiv of **12** with 1 equiv of **14** in methanol (comproportionation) affords violet crystals of $[L_2Ni_3](PF_6)$ (**13**), and oxidation of **14** with 1 equiv of $[Ni^{III}(tacn)_2](ClO_4)_3$ in methanol yields $[L_2Ni_3](PF_6)_3$ (**15**).

Electrochemistry. The results of the electrochemical investigation are summarized in Table 2. In the following, all redox potentials are referenced in volts *versus* the ferrocenium/ferrocene couple (Fc^+/Fc).

The cyclic voltammograms of the mononuclear species $[LCo^{III}]$ and of the trinuclear complex $[L_2Co^{III}_3](PF_6)_3$ (**2**) are displayed in Figure 1. As noted previously,[10] the N_3S_3 donor set in $[LCo^{III}]$ stabilizes the trivalent oxidation state enormously; the $[LCo^{II}]^-$ species is not accessible to potentials as negative as −1.9 V. On the other hand, an irreversible oxidation wave at +0.30 V and a corresponding irreversible reduction at −1.6 V are assigned to ligand rather than metal centered electron transfer waves. It is therefore important to note that trinuclear **2** is redox-inactive in the range −0.5 to +1.1 V. Thus, ligand centered oxidations are not observed for **2**. A tentative interpretation for the oxidative process of $[LCo^{III}]$ involves intramolecular disulfide formation[10] (2e oxidation of two thiophenolato groups) which is not feasible in **2** due to the bridging mode of the thiophenolate ligands.

The central Co^{III} of **2** in a CoS_6 environment is reversibly one-electron reduced at $E_{1/2} = -0.65$ V. A similar electrochemical process has been reported for *rac*-$[Co^{III}\{Co^{III}(aet)_3\}_2]^{3+}$ [31] where aet represents 2-aminoethanethiolate, $H_2NCH_2CH_2S^-$, and for $[Co^{III}\{Rh^{III}(aet)_3\}_2]^{3+}$.[20] At a very negative potential of −1.35 V the terminal Co^{III} ions of **2** are irreversibly reduced.

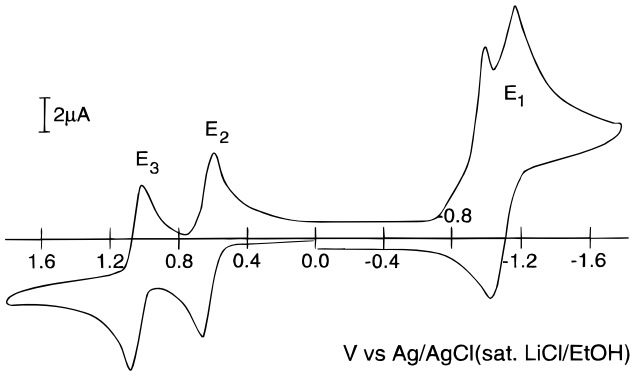

Figure 2. Cv of $[\{LCo^{III}\}_2Ni^{II}](PF_6)_2$ (**3**) in acetonitrile. Conditions are as given in Figure 1.

Replacement of the central Co^{III} in **2** by Ni^{II} gives the dicationic complex **3** the cv of which is shown in Figure 2. From acetonitrile solutions of **4** and **5**, identical cv's have been obtained. In the potential range −1.2 to +1.1 V two reversible one-electron transfer waves are detected at $E_{1/2} = +0.11$ and +0.52 V. Coulometric measurements first at 0.3 V and then at 0.75 V establish two subsequent one-electron oxidation steps for **3**. During these oxidation processes the original brown color of a solution of **3** changes first to blue and then to violet. These oxidations are believed to be metal-centered involving the central Ni^{II} ion in **3** and are assigned as in eq 2.

$$\underset{\mathbf{3}}{[\{LCo^{III}\}_2Ni^{II}]^{2+}} \underset{+e}{\overset{-e}{\rightleftharpoons}}_{E^2} \underset{\mathbf{4}}{[\{LCo^{III}\}_2Ni^{III}]^{3+}} \underset{+e}{\overset{-e}{\rightleftharpoons}}_{E^3} \underset{\mathbf{5}}{[\{LCo^{III}\}_2Ni^{IV}]^{4+}} \quad (2)$$

At more negative potentials <−1.3 V irreversible reduction processes are observed which were not investigated in detail because they show a dependence on the nature of working electrode and scan rate.

The cv of **6** dissolved in CH_3CN containing 0.10 M tetra-*n*-butylammonium hexafluorophosphate as supporting electrolyte is shown in Figure 3 (top). Three one-electron transfer waves are detectable of which two ($E^1 = -0.32$ V and $E^2 = 0.09$ V) are reversible whereas the third at $E^3 = 0.72$ V is quasireversible; eq 3.

$$\underset{\mathbf{6}}{[\{LNi^{II}\}_2Co^{III}]^{+}} \underset{+e}{\overset{-e}{\rightleftharpoons}}^{E^1} \underset{\mathbf{7}}{[\{LNi\}_2Co^{III}]^{2+}} \underset{+e}{\overset{-e}{\rightleftharpoons}}^{E^2} \underset{\mathbf{8}}{[\{LNi\}_2Co^{III}]^{3+}} \underset{+e}{\overset{-e}{\rightleftharpoons}}^{E^3} [\{LNi\}_2Co^{III}]^{4+} \quad (3)$$

The linkage isomer of **6** namely complex **9** with a $[LNi^{II}\text{-}Ni^{II}Co^{III}L]^+$ cation shows also three one-electron transfer waves, two of which are reversible (E^1 and E^2) and one quasireversible (E^3): $E^1 = -0.40$ V, $E^2 = 0.095$ V, $E^3 = 0.64$ V. Figure 3 (bottom) displays this cv. Note that these redox potentials are similar but not identical to those observed for **6**. Assignment of these processes is as in eq 4.

$$\underset{\mathbf{9}}{[LNiNiCo^{III}L]^{+}} \underset{+e}{\overset{-e}{\rightleftharpoons}}^{E^1} \underset{\mathbf{10}}{[LNiNiCo^{III}L]^{2+}} \underset{+e^-}{\overset{-e^-}{\rightleftharpoons}}^{E^2} \underset{\mathbf{11}}{[LNiNiCo^{III}L]^{3+}} \underset{+e^-}{\overset{-e}{\rightleftharpoons}}^{E^3} [LNiNiCo^{III}L]^{4+} \quad (4)$$

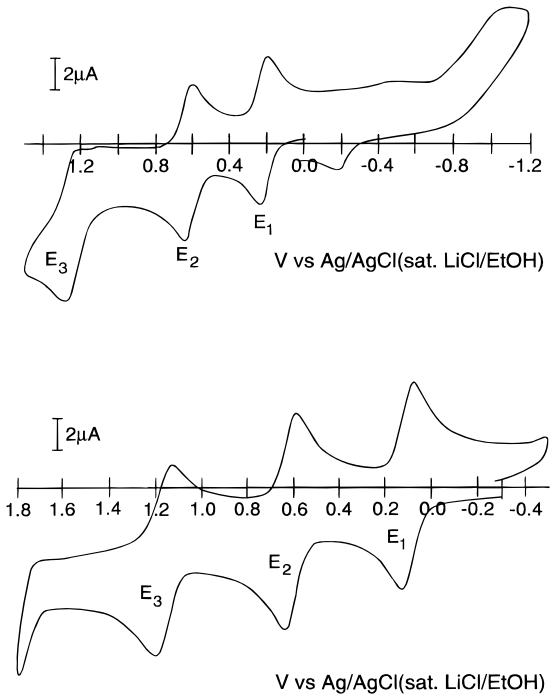

Figure 3. Cv of $[\{LNi^{II}\}_2Co^{III}](PF_6)$ (**6**) (top) and $[LNi^{II}Ni^{II}Co^{III}L](PF_6)$ (**9**) (bottom) in CH_3CN. Conditions are as given in Figure 1.

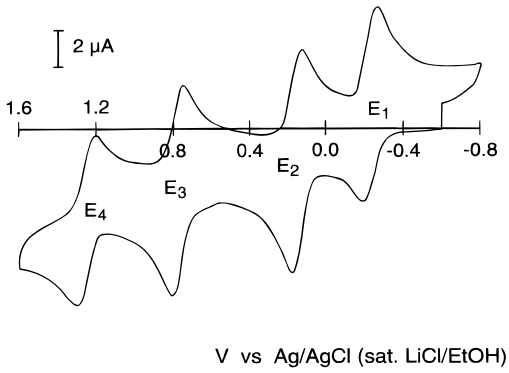

Figure 4. Cv of $[\{LNi\}_2Ni](PF_6)_2$ (**14**) in CH_3CN. Conditions are as given in Figure 1.

The cv's of the isolated oxidation products **10** and **11** are again identical with that of **9**.

Figure 4 exhibits the cv of the trinuclear dicationic Ni^{II} complex **14**. It has not been possible to record the cv of **12** due to its low solubility in all common solvents. Three reversible (E^1−E^3) and one quasireversible (E^4) one-electron transfer waves are clearly detected at $E^1 = -0.76$ V, $E^2 = -0.38$ V, $E^3 = 0.24_5$ V; and $E^4 = +0.71$ V which are assigned as shown in eq 5.

$$\underset{\mathbf{12}}{[\{LNi\}_2Ni]^0} \overset{E^1}{\underset{+e}{\rightleftharpoons}} \underset{\mathbf{13}}{[\{LNi\}_2Ni]^+} \overset{E^2}{\underset{+e}{\rightleftharpoons}} \underset{\mathbf{14}}{[\{LNi\}_2Ni]^{2+}} \overset{E^3}{\underset{+e}{\rightleftharpoons}} \underset{\mathbf{15}}{[\{LNi\}_2Ni]^{3+}} \overset{E^4}{\underset{+e^-}{\rightleftharpoons}} [\{LNi\}_2Ni]^{4+} \quad (5)$$

The cv's of **13** and **15** are again identical to that of **14**. Interestingly, after two successive coulometric reductions of **14** dissolved in CH_3CN a colorless solution was obtained and complete deposition of **12** on the working Pt-gauze electrode was observed. Two electrons per dication are necessary for this process and these were determined coulometrically.

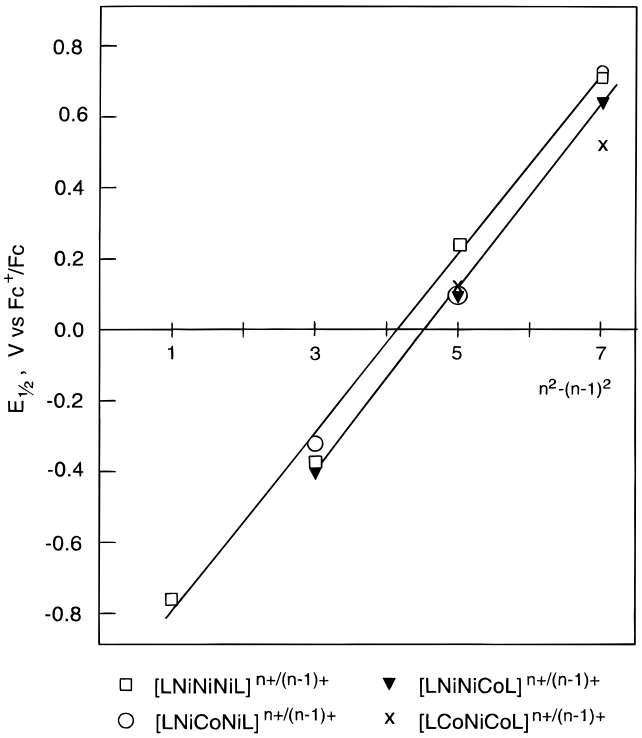

Figure 5. Plot of the redox potential, $E_{1/2}$ *vs* $n^2 - (n-1)^2$ where n is the charge of a trinuclear complex $[\{LM^1\}_2M^2]^{n+}$.

It is interesting that the difference between two redox potentials, $E_{1/2}{}^n - E_{1/2}{}^{n-1}$, of redox couples $[\{LM^1\}_2M^2]^{n+/(n-1)+}$ is nearly invariably ∼400 mV irrespective of the nature of the trinuclear complex. A very simple electrostatic model taking into account only the difference of the solvation energy of a species carrying an $n+$ and an $(n-1)+$ charge can be developed by using the Born equation[32] for a charged spherical particle of radius r in a medium with a dielectricity constant ϵ_E, eq 6

$$-\Delta G^\circ = E^f F = n^2 e^2 N_L / 8\pi r \epsilon_0 \epsilon_E \quad (6)$$

where E^f represents the redox potential in volts, N_L is the Avogadro number and F the Faraday constant, $8\pi r$ is a geometric parameter of the spherical particle, $\epsilon_0\epsilon_E$ is the dielectricity constant of the surrounding medium, and ne is the electric charge of the particle. Assuming that the difference of the redox potentials $[L_2M_3]^{n+/(n-1)+}$ ($n = 4, 3, 2, 1$) is primarily governed by the differing solvation energy of two charged cations one can derive eq 7.

$$\Delta E^f = (2n-1)(e^2 N_L / 8\pi r \epsilon_0 \epsilon_E) F^{-1} \quad (7)$$

This simple model predicts that a plot of the measured redox potentials for an $[L_2M_3]^{n+}$ species *versus* $n^2 - (n-1)^2 = 2n - 1$ should be linear with a slope $k = (e^2 N_L / 8\pi r \epsilon_0 \epsilon_E) F^{-1}$. This is indeed the case as Figure 5 shows for the series of complexes **6**−**8**, **9**−**11**, and **12**−**15**. It is even more surprising that the slope for each type of complex is very similar regardless of the fact that different hetero- and homotrinuclear series of complexes are involved. This slope k is ∼250 mV.

To a first approximation the trinuclear species may be regarded as spherical with a radius $r = 4.0$ Å. The $N_3M(\mu\text{-}S)_3M(\mu\text{-}S)_3MN_3$ core is surrounded by an aliphatic and aromatic hydrocarbon sphere for which a dielectricity constant ϵ_E of 2 is estimated. The pure solvent acetonitrile has an ϵ_E of 36 which

(32) Born, M. *Z. Phys.* **1920**, *1*, 45.

is considerably lowered by the supporting electrolyte tetra-*n*-butylammonium hexafluorophosphate. Assuming an effective dielectricity constant of 7 and a radius of 4.0 Å we calculate the slope *k* to be 250 mV by using eq 7. We realize that the excellent agreement between the calculated and experimentally observed value for the slope *k* may be fortuitous especially when considering the crudeness of the model but it does imply that it is not possible to identify localized electron transfer processes at a single metal ion site in $[L_2M_3]^{n+}$ complexes. Thus, the electrochemistry points to electronically delocalized cores. Similar analyses have been applied to the effects of solvent and protein dielectric on the redox potentials of iron−sulfur clusters.[33]

Solid-State Molecular Structures of [{LNi}$_2$Ni]BPh$_4$ (13*) and [{LNi}$_2$Ni](PF$_6$)$_2$·5acetone (14). The crystal structure of **13*** consists of trinuclear monocations $[\{LNi\}_2Ni]^+$ and well-separated tetraphenylborate anions. Figure 6 displays the structure of the monocation which possesses S_6 symmetry where the central nickel ion lies on a crystallographic inversion center. Table 3 summarizes selected bond distances and angles of the $N_3Ni(S)_3Ni(S)_3NiN_3$ core. Six thiophenolate sulfur atoms of two ligand sets, L^{3-}, bind to two terminal nickel ions (N_3S_3 donor set) and a nickel ion in the central position (S_6 donor set) giving rise to a core structure of three face-sharing octahedra.

The stereochemistry of this trinuclear species is interesting since there are three different sources of chirality. First, the conformation of the three five-membered chelate rings Ni−N−C−C−N of the coordinated 1,4,7-triazacyclononane backbone of the terminal nickel ions is either ($\lambda\lambda\lambda$) or ($\delta\delta\delta$). As in all crystal structures of complexes containing the (1,4,7-triazacyclononane)metal fragment conformational mix, e.g. ($\lambda\delta\delta$) or ($\lambda\lambda\delta$), has not been observed. Secondly, in octahedral complexes containing a macrocyclic ligand with three pendent arms Λ or Δ configuration of the N_3S_3M core is possible. In the present case the terminal nickel ions exist in the enantiomeric forms Δ($\lambda\lambda\lambda$) and Λ($\delta\delta\delta$). This has also been observed crystallographically for the mononuclear complexes $[LCo^{III}]$[10] and $[LFe^{III}]$[9]. Finally, in a trinuclear face-sharing octahedral structure as discussed here, there are, in principle, two diastereomeric forms conceivable where (i) both terminal nickel atoms have the same configuration Δ($\lambda\lambda\lambda$)···Δ($\lambda\lambda\lambda$) and its enantiomer or (ii) a different one as in Δ($\lambda\lambda\lambda$)···Λ($\delta\delta\delta$) which is achiral. A simple consideration of the stereochemical requirements of the six tertiary butyl groups in LMMML complexes shows that the Δ($\lambda\lambda\lambda$)···Δ($\lambda\lambda\lambda$) form leads to serious spatial congestion of these bulky groups as they are eclipsed. Only the staggered configuration of the tertiary butyl groups in Δ($\lambda\lambda\lambda$)···Λ($\delta\delta\delta$) leads to a stable, sterically not crowded situation. Thus, for all complexes of the $[LMMML]^{n+}$ type only one achiral stereoisomer needs to be considered. This is in contrast to similar complexes containing the sterically less demanding aminoethanethiolate ligand as in $[(aet)_3Co^{III}Co^{III}Co^{III}(aet)_3]^{3+}$ of which three stereoisomers have been synthesized and characterized.[16,18−20,22,31]

The metrical details of the $N_3Ni(\mu\text{-}S)_3Ni(\mu\text{-}S)_3NiN_3$ core in **13*** are briefly discussed in the following (Table 4). The average Ni−N bond distance of 2.096 Å corresponds nicely to that of 2.10 Å reported for $[Ni^{II}(tacn)_2](NO_3)Cl\cdot H_2O$.[34] In the Jahn−Teller distorted $Ni^{III}N_6$ octahedron of $[Ni^{III}(tacn)_2]_2(S_2O_6)_3\cdot 7H_2O$ the average Ni^{III}−N bond lengths in transaxial position are 2.110(5) and 1.971(5) Å in the basal plane (overall average 2.017 Å).[28b] This would point to the assignment of a +II oxidation state at the terminal nickel ions in **13***. On the other hand, the average Ni−S distances of 2.361 Å at the terminal nickel ions and of 2.373 Å at the central nickel ion are not significantly different to allow unambiguously such an

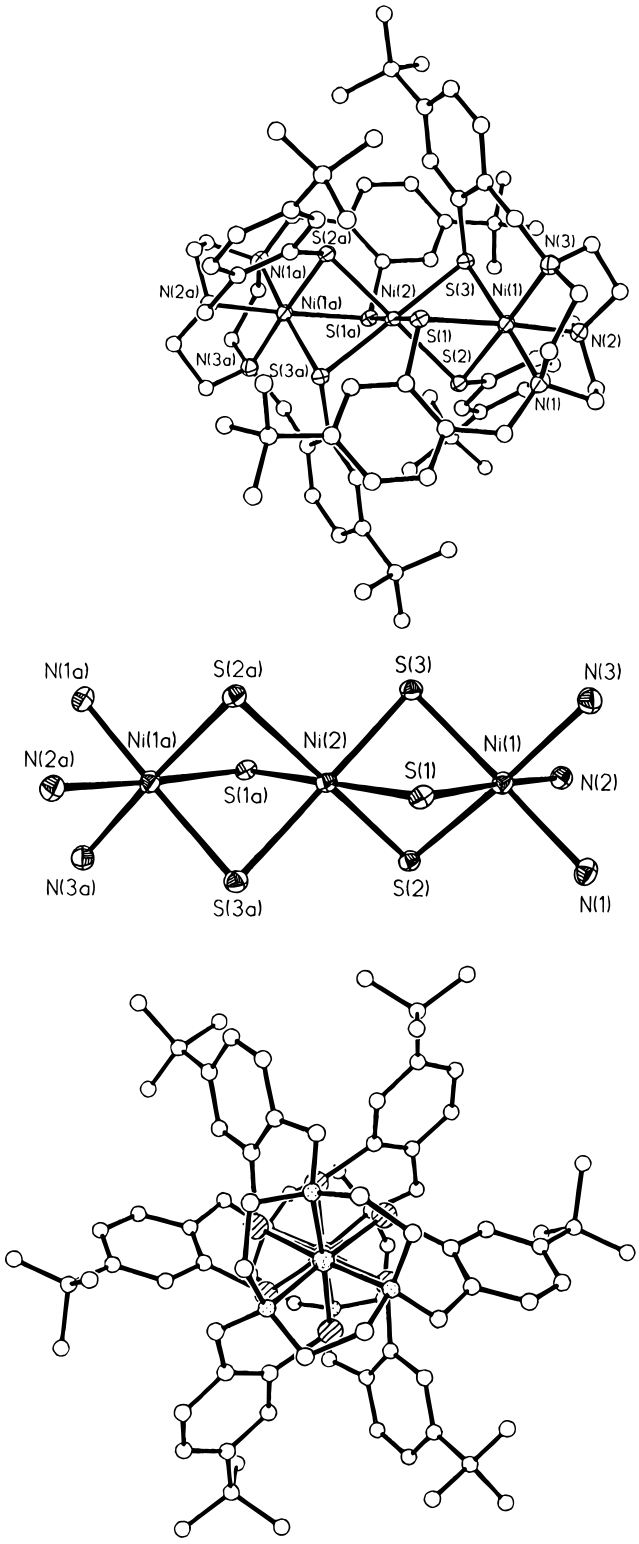

Figure 6. Structure of the monocation in crystals of **13***. Top: Side view. Middle: view of the $N_3Ni(\mu\text{-}S)_3Ni(\mu\text{-}S)_3NiN_3$ core. Bottom: view down the Ni···Ni···Ni threefold axis emphasizing the staggered configuration of thiophenolate pendent arms. The structure of the dication in crystals of **14*** is very similar and is not shown. The same atom labels apply.

(33) (a) Kassner, R. J. *J. Am. Chem. Soc.* **1973**, *95*, 2674. (b) Kassner, R. J.; Yang, W. *J. Am. Chem. Soc.* **1977**, *99*, 4351. (c) Kodaka, M.; Tomohiro, T.; Okuno, H. (Y.) *J. Phys. Chem.* **1991**, *95*, 6741.

(34) Zompa, L. J.; Margulis, T. N. *Inorg. Chim. Acta* **1978**, *28*, L157.

Table 3. Selected Bond Distance (Å) and Angles (deg) of the Monocation in Crystals of **13*** and in Parentheses of the Dication in **14**

Ni1−S1	2.353(3)	(2.358(1))	Ni1−S2	2.368(3)	(2.353(1))
Ni1−S3	2.361(3)	(2.353(1))	Ni1−Ni1	2.079(9)	(2.083(4))
Ni1−N2	2.10(1)	(2.081(4))	Ni1−N3	2.110(8)	(2.100(4))
Ni2−S1	2.371(3)	(2.326(1))	Ni2−S2	2.386(3)	(2.324(1))
Ni2−S3	2.363(3)	(2.328(1))	S1−C9	1.72(1)	(1.777(4))
S2−C20	1.75(1)	(1.773(4))	S3−C31	1.74(1)	(1.774(4))
Ni1···Ni2	3.008(2)	(3.029(1))			
S1−Ni1−S2	83.9(1)	(82.24(4))	S1−Ni1−S3	84.1(1)	(81.85(4))
S2−Ni1−S3	84.6(1)	(81.97(4))	S1−Ni1−N1	93.6(3)	(94.4(1))
S2−Ni1−N1	175.9(3)	(176.1(1))	S3−Ni1−N1	98.4(3)	(98.2(1))
S1−Ni1−N2	98.8(3)	(98.9(1))	S2−Ni1−N2	92.7(3)	(94.8(1))
S3−Ni1−N2	175.8(3)	(176.8(1))	N1−Ni1−N2	84.4(4)	(85.0(2))
S1−Ni1−N3	176.3(3)	(176.3(1))	S2−Ni1−N3	98.1(3)	(98.4(1))
S3−Ni1−N3	93.0(3)	(94.5(1))	N1−Ni1−N3	84.5(4)	(85.4(2))
N2−Ni1−N3	84.2(4)	(84.7(1))	S1−Ni2−S2	83.2(1)	(83.1(3))
S1−Ni2−S3	83.7(1)	(83.1(3))	S2−Ni2−S3	84.2(1)	(83.6(3))
S3−Ni2−S1A	96.3(1)	(96.4(3))	S2−Ni2−S1A	96.8(1)	(96.9(4))
Ni1−S1−Ni2	79.1(1)	(80.6(3))	S3−Ni2−S2A	95.8(1)	(96.9(3))
Ni1−S3−Ni2	79.1(1)	(80.6(3))	Ni1−S2−Ni2	78.5(1)	(80.7(3))

assignment. The fact that the Ni−S distances are within experimental error identical and the absence of a significant Jahn−Teller distortion expected for a localized Ni^{III} ion with low spin d^7 electron configuration may point to be a delocalized mixed valent form of the monocation in **13***. In the crystal structure of $[\{Co^{III}(aet)_3\}_2Ni^{II}]Cl_2\cdot 3H_2O$[23] the central octahedral Ni^{II} is coordinated to six bridging mercapto sulfur atoms at an average Ni^{II}−S distance of 2.400 Å which is longer by only 0.027 Å than in complex **13***.

We have also solved the crystal structure of $[LCo^{III}Co^{II}Co^{III}L][\{Co^{II}Cl_2H_2O\}_2(\mu\text{-}Cl)](PF_6)\cdot$unknown solvent,[35] the full details of which will be reported elsewhere. The LCo^{III} fragment has average Co−N and Co−S distances of 2.003 and 2.242 Å, respectively. Interestingly, the central cobalt(II) ion has three pairwise different Co−S distances at 2.264(1), 2.278(1), and 2.289(1) Å which may be a manifestation of a tetragonal Jahn−Teller distortion of a localized Co(II) ion. Note that the average Co^{II}−S distance of the central cobalt ion at 2.277 Å is only slightly longer than the corresponding Co^{III}−S bond at 2.262(11) Å in $[\{Co(aet)_3\}_2Co^{III}]_2(SO_4)Cl_4$.[21]

The Co···Co distance is 3.034 Å and the average Co−S−Co angle is 84.4°, whereas the two adjacent nickel ions in **13*** are separated by 3.008 Å and the average Ni−S−Ni bond angle is 78.9°. We take this as an indication that no direct through-space Ni···Ni bonding occurs in **13***.[36] In the above $[\{Co^{III}(aet)_3\}_2Ni^{II}]Cl_2\cdot 3H_2O$ analog[23] the average Co···Ni distance is at 2.930(1) Å and the average Co−S−Ni bond angle is 78° (Table 4).

The structure of the dication $[\{LNi\}_2Ni]^{2+}$ in **14** is very similar to that of the monocation in **13***. It is quite remarkable and significant that the metrical details of the LNi fragment in both structures are identical within experimental error. Thus one electron oxidation of **13** to **14** results in a small contraction of the Ni−S bonds of the central nickel ion (2.373 Å in **13*** and 2.326 Å in **14**) only. It is therefore justified to assign the distribution of oxidation states in **13** as $[LNi^{II}Ni^{III}Ni^{II}L]^+$ and in **14** as $[LNi^{II}Ni^{IV}Ni^{II}L]^{2+}$. On the other hand, the Ni−S bond length difference Δ between the $Ni^{II}S^6$ octahedron in $[K(2,2,2\text{-crypt})][Ni^{II}(S_2CPh)_3]$[37] and the $Ni^{IV}S_6$ octahedron in $[Ni^{IV}(n\text{-}Bu_2Dtc)_3]Br$[38] (where *n*-$Bu_2$Dtc is *N*,*N*-di-*n*-butyl dithiocarbamate) is 0.16 Å, whereas for **13** and **14** this difference is only 0.074 Å.

Electronic Structure of Complexes. Variable-temperature magnetic susceptibilities of complexes were measured in the range 2−295 K by using a SQUID magnetometer and an applied external magnetic field of 1.0 T. The experimental data, χ_{exp}, were converted to the molar paramagnetic susceptibility, χ_M, by correcting for underlying diamagnetism, χ_D, and temperature-independent paramagnetism, χ_{TIP}. χ_D was calculated by use of Pascal's tabulated constants and χ_{TIP} was a fit parameter in the subsequent simulation and fitting procedures. The effective magnetic moments, μ_{eff}, of complexes **6**−**8** as a function of the temperature are shown in Figure 7, those of **9**−**11** in Figure 8, those of **12**−**15** in Figure 9, and those of complex **1** in Figure 11.

We have employed the following fitting procedure for the $\chi_M T$ data as a function of the temperature T to the spin Hamiltonian eq 1 including a Zeeman term $\sum_{i=1}^{n}\mu_B B g S_i$ and a term correcting for an unknown paramagnetic impurity p with $S = 1$ or $^3/_2$. In order to reduce the number of variables, the g values for paramagnetic metal ions were considered to be identical irrespective of their differing ligand environments and oxidation states. With the exception of **1**, the simulations did not show indications of significant zero-field splittings and, consequently, the corresponding terms were not included in eq 1. For **1** the conventional zero-field term with D and E/D were included in eq 1. The assumption that zero-field splittings in the series **2**−**15** are in general weak ($D \lesssim 1$ cm^{-1}) is corroborated by the EPR spectra of **7**, **10**, **13**, and **15** shown in Figure 10. Only for **7** is an EPR pattern with resolved signals at distinct g values observed as is expected for cases with $D \gg h\nu$ (∼0.3 cm^{-1} at X-band). All other complexes display spectra which are more or less perturbed by the effect of competing zero-field and Zeeman interactions ($D \approx h\nu$).

The results of the simulations are summarized in Table 5. As indicated above, χ_{TIP} is a fit parameter and, consequently, there is considerable scatter of these values ((100−2600) 10^{-6} cm^3 mol^{-1}) in the series **2**−**15**. Possible ambiguities of the results were excluded by systematic searches of the fit parameter space including χ_{TIP}. In order to do this we have calculated fit-error contour maps for J_t *vs* χ_{TIP} and J_a *vs* J_t to ensure the global nature of the fit minima obtained. No significant covariances of parameters were found in the vicinity of the fit minima. From the error contour maps and visual inspection of calculated $\mu_{eff}(T)$ curves we estimate typical errors of χ_{TIP} as well as for J_a and J_t of ∼10%.

For complexes **3**, **4**, and **5**, containing a single central nickel ion and two terminal diamagnetic LCo^{III} units, the temperature-independent effective magnetic moment of 2.95 μ_B was calculated for **3**, whereas μ_{eff} is 1.82 μ_B for **4** in the range 5−300 K, and for **5** in the temperature range 80−300 K a temperature-independent paramagnetism of $\chi_{TIP} = 840 \times 10^{-6}$ cm^3 mol^{-1} (emu) was experimentally found. Thus, $S = 1$, $^1/_2$, and 0 ground states for **3**, **4**, and **5**, respectively, are observed in agreement with the assignment to a single octahedral $Ni^{II}(d^8)$ in **3**, low-

(35) Preliminary data of the crystal structure determination of $[\{LCo^{III}\}_2Co^{II}][Co^{II}_2Cl_5(H_2O)_2](PF_6)\cdot$unknown solvent: monoclinic, space group $C2/c$ (No. 15), $a = 28.275(9)$ Å, $b = 17.876(8)$ Å, $c = 19.636(8)$ Å, $\beta = 104.3(5)°$, $V = 9619.0$ Å^3, $\rho_{calc} = 1.43$ g cm^{-3}; $Z = 4$; μ = (Mo Kα) = 0.66 mm^{-1}, 6373 unique reflections with $F_o > 4.0\sigma(F_o)$ were used in the refinement of 589 parameters, $R = 0.078$.

(36) A few mixed-valent Ni(III)Ni(II) dinuclear complexes with four or five coordinate nickel ions and thiolate bridges have been characterized by X-ray crystallography. One of these contains an Ni···Ni bond: (a) $[Pr_4N][Ni_2\{P(o\text{-}C_6H_4S)_3\}_2]$: Ni−Ni 2.501(2) Å; Franolic, J. D.; Wang, W. Y.; Millar, M. *J. Am. Chem. Soc.* **1992**, *114*, 6587. In contrast, see: (b) $[Ni_4(S\text{-}i\text{-}C_3H_7)_8I]$: Ni···Ni 4.111 Å; Krüger, T.; Krebs, B.; Henkel, G. *Angew. Chem.* **1992**, *104*, 71; *Angew. Chem., Int. Ed. Engl.* **1992**, *31*, 54.

(37) Fackler, J. P.; Del Niera, R.; Campana, C.; Trzcinska-Bancroft, B. *J. Am. Chem. Soc.* **1984**, *106*, 7883.

(38) Fackler, J. P.; Avdeef, A.; Fischer, R. G., Jr. *J. Am. Chem. Soc.* **1973**, *95*, 774.

Table 4. Comparison of Structural Data of Complexes[a]

complex	M_t−S, Å	M_t−N, Å	M_c−S, Å	$M_t\cdots M_c$, Å	M_t−S−M_c, deg	ref
$[Ni^{IV}(n\text{-}Bu_2Dtc)_3]Br$			2.261			
$[K(2,2,2\text{-crypt})][Ni^{II}(S_2CPh)_3]$			2.42			
$[LCo^{III}]$	2.24	2.04				
$[\{LCo^{III}\}_2Co^{II}][Co_2Cl_5(H_2O)_2](PF_6)$	2.241	2.003	2.277	3.034	84.4	this work
$[\{L'_3Co^{III}\}_2Co^{III}]_2(SO_4)Cl_4$	2.238	1.996	2.262	2.857	78.8	21
$[\{L'_3Co^{III}\}_2Ni^{II}]Cl_2\cdot 3H_2O$	2.253	2.005	2.400	2.930	78.3	23
$[\{LNi\}_2Ni][BPh_4]$ (**13***)	2.361	2.096	2.373	3.008	78.9	this work
$[\{LNi\}_2Ni](PF_6)_2$ (**14**)	2.355	2.088	2.326	3.029	80.6	this work
$[\{(L\text{-}cys)_3Co^{III}\}_2Co^{III}](NO_3)_2\cdot 5H_2O$	2.231	2.008	2.258	2.856	79.4	22

[a] Abbreviations: *n*-Bu_2Dtc = *N*,*N*-di-*n*-butyldithiocarbamato; 2,2,2-crypt = 4,7,13,16,21,24-hexaoxa-1,10-diazabicyclo[8.8.8]hexacosane; S_2CPh = dithiobenzoate; L = tris(4-*tert*-butyl-2-mercaptobenzyl)-1,4,7-triazacyclononane; L′ = 2-aminoethanethiolate; L-cys = L-cysteinate; M_t = metal (terminal); M_c = metal (central).

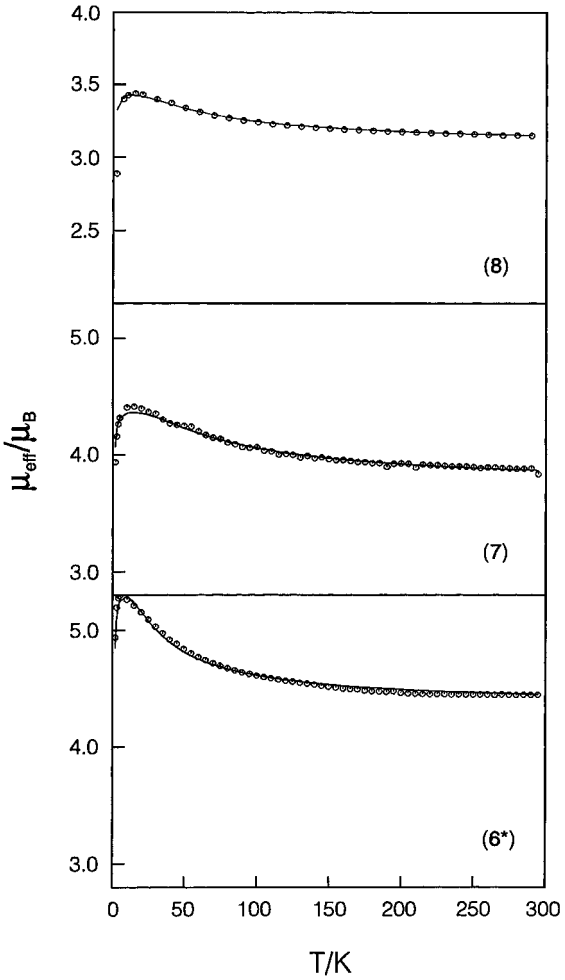

Figure 7. Temperature dependence of the magnetic moments of complexes $[LNiCo^{III}NiL]^{+/2+/3+}$ **6***, **7**, and **8**. The solid lines represent a best fit of data to the isotropic Heisenberg−Dirac−van Vleck model (see text).

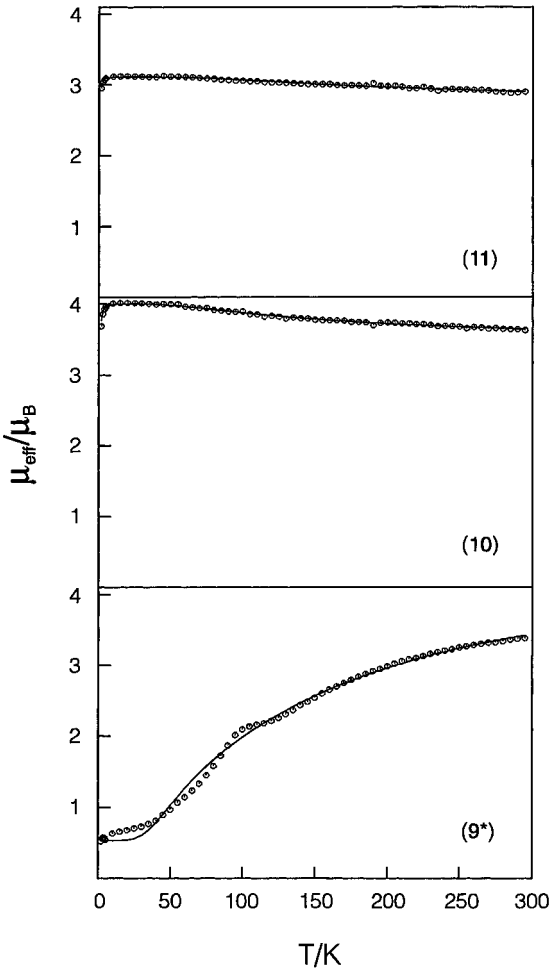

Figure 8. Temperature dependence of the magnetic moments of $[LNiNiCo^{III}L]^{+/2+/3+}$ complexes **9** (bottom), **10** (middle), and **11** (top).

spin $Ni^{III}(d^7)$ in **4**, and a low-spin $Ni^{IV}(d^6)$ in **5**. The presence of a Ni^{III} ion in **4** was corroborated by its X-band EPR spectrum measured in acetonitrile at 2.7 K which exhibits an anisotropic signal with *g* values of 2.11, 2.09, and 2.04.

In complexes **6***, **7**, and **8** a central cobalt ion is always coordinated via six thiophenolate bridges to two paramagnetic terminal LNi entities. Simple charge considerations imply that in the monocation of **6*** the oxidation state distribution is $[LNi^{II}Co^{III}Ni^{II}L]^+$. The fit for **6*** to the Heisenberg−Dirac−van Vleck (HDvV) model for dinuclear complexes ($S_1 = S_2 = 1$) yielded a *ferromagnetic* coupling constant $J_t = +7$ cm^{-1} and $g = 2.2$. Thus, **6*** has an $S = 2$ ground state.

One-electron oxidation of **6** yields the dication **7**. Since it is difficult to envisage the generation of a Co^{IV} ion, one of the two $[LNi^{II}]^-$ entities in **6** must be oxidized to produce a mixed-valent compound $[LNi^{II}Co^{III}Ni^{III}L]^{2+}$. An excellent fit of the magnetic data employing the HDvV model ($S_1 = 1$ and $S_2 = {}^1/_2$) yields a J_t value of +20 cm^{-1} and $g = 2.3$. The dication in **7** possesses an $S = {}^3/_2$ ground state. This is corroborated by the X-band EPR spectrum of **7** in CH_3CN solution shown in Figure 10. At 2.8 K an axial spectrum with $g_\perp = 4.0$ and $g_\parallel = 2.04$ is indicative of an $S_t = {}^3/_2$ ground state.

The magnetism of complex **8** can be interpreted in terms of a ferromagnetically coupled $[LNi^{III}Co^{III}Ni^{III}L]^{3+}$ system ($S_1 = S_2 = {}^1/_2$). The HDvV model produces a reasonable fit to the data with the parameters $J_t = +26$ cm^{-1}, $g = 2.4$ including a paramagnetic impurity of 18% with $S = {}^3/_2$. Thus, **8** has an $S = 1$ ground state. Attempts to prepare a purer sample have failed.

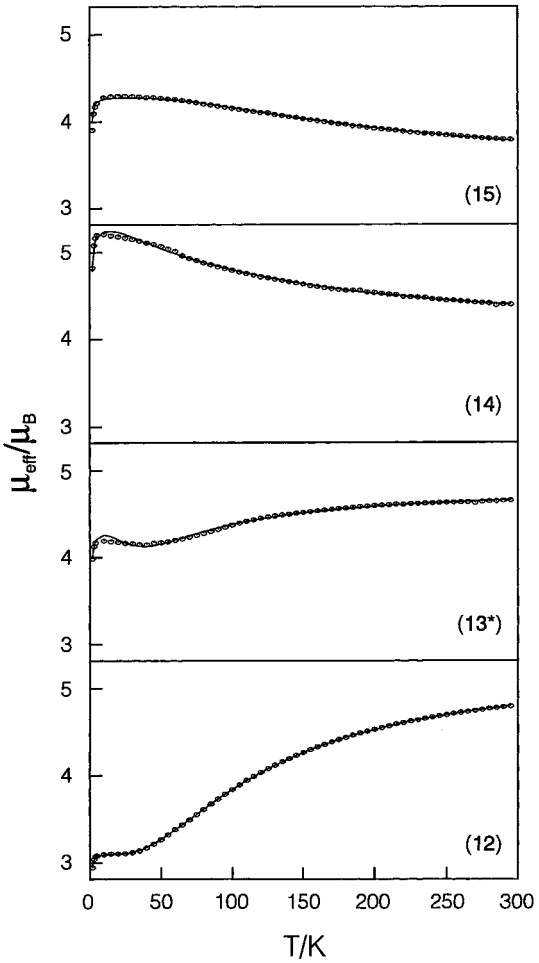

Figure 9. Temperature dependence of the magnetic moments of $[LNiNiNiL]^{0/1+/2+/3+}$ complexes **12**, **13**, **14**, and **15**.

The linkage isomer of **6*** is complex **9*** where two octahedral nickel(II) ions are in adjacent positions relative to each other: $[LNi^{II}Ni^{II}Co^{III}L]^{+}$. Complex **9*** possesses an $S = 0$ ground state. Within the HDvV formalism an intramolecular *antiferromagnetic* exchange interaction between the two Ni^{II} ions yields the parameters $J_a = -61$ cm^{-1}, $g = 2.2$, and a paramagnetic impurity with $S = 1$ (3.2%). Note that the linkage isomer **6*** $[LNi^{II}Co^{III}Ni^{II}L]^{+}$ possesses an $S = 2$ ground state. Thus, the magnetic properties of **6*** and **9*** are dramatically different.

Removal of one electron from the monocation **9*** yielding dicationic **10** also has a drastic effect on the magnetic properties. By using the HDvV model we obtain a good fit with $J = +41$ cm^{-1} and $g = 2.1$ with $S_1 = 1$, $S_2 = {}^1/_2$. The X-band EPR spectrum of **10** in CH_3CN at 2.8 K (Figure 10) confirms the $S_t = {}^3/_2$ ground state. A rhombic signal with $g_x = 3.6$, $g_y = 4.6$, and $g_z = 2.1$ is observed. Note that a one-electron oxidation of **9*** yielding **10** changes the sign of the coupling constant.

It is possible to fit the magnetic data of complex **11** to the HDvV model assuming the presence of two Ni^{III} with $S_1 = S_2 = {}^1/_2$: $J = +81$ cm^{-1} and $g = 2.2$. Thus, the $S = 1$ ground state would be attained by a strong ferromagnetic coupling between two adjacent low-spin Ni^{III} ions.

For **12**, a decrease of the magnetic moment from 4.78 μ_B at 295 with decreasing temperature is observed until a plateau is reached at 3.10 μ_B at 30 K (Figure 9, bottom). This clearly indicates an $S = 1$ ground state for **12**, which is attained by an antiferromagnetic coupling between two adjacent Ni^{II} ions ($J_a = -28$ cm^{-1}). Similarly, in **13*** the magnetic moment also decreases with decreasing temperature to a plateau of 4.15 μ_B at 50 K (antiferromagnetic coupling) indicating an $S = {}^3/_2$ ground state. This is corroborated by the X-band EPR spectrum of a solid sample of **13** at 10 K shown in Figure 10 which exhibits a rhombic signal with $g_x = 5.85$, $g_y = 2.45$, and $g_z = 1.64$.

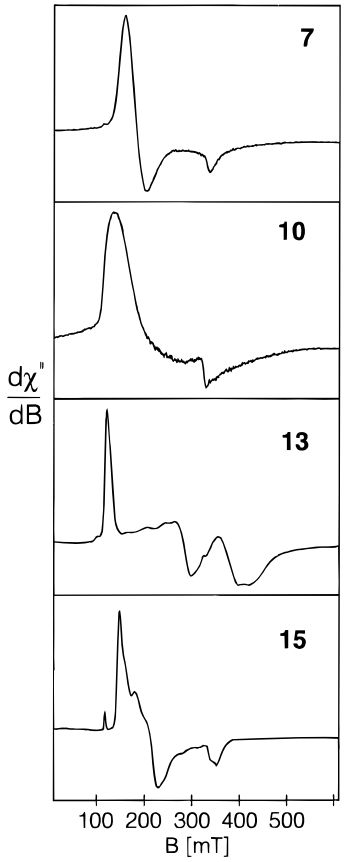

Figure 10. X-Band EPR spectra of complexes **7** at 1.5 K, **10** at 2.8 K, and **15** at 10 K in CH_3CN solution and of a solid sample of **13** at 4 K. (Conditions: $\nu = 9.64$ GHz for **7**, **10**, **15**, and $\nu = 9.47$ GHz for **13**; microwave power 20 (**7**, **10**, **15**) and 0.2 mW (**13**); modulation amplitude in gauss and in parentheses modulation frequency in kHz: **7**, 11.431 (100); **10**, 11.431 (12.5); **15**, 11.431 (100); **13**, 19.749 (100)).

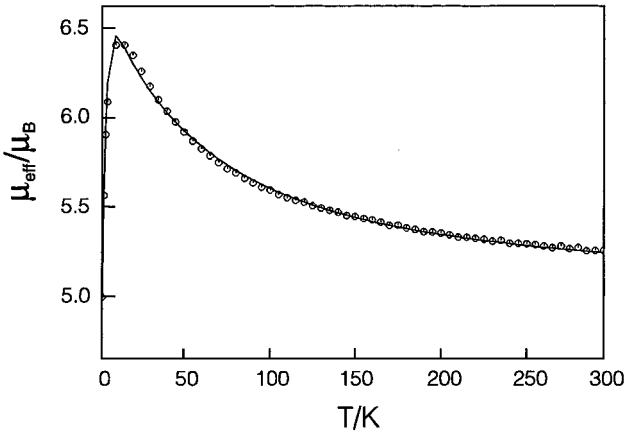

Figure 11. Temperature dependence of the magnetic moment of **1**.

In order to fit the magnetic data of **14** to the HDvV model three different distributions of oxidation states were considered, namely $[LNi^{III}Ni^{III}Ni^{II}L]^{2+}$, $[LNi^{III}Ni^{II}Ni^{III}L]^{2+}$, and $[LNi^{II}Ni^{IV}Ni^{II}L]^{2+}$. Note that the asymmetric $Ni^{III}Ni^{III}Ni^{II}$ form requires *three* different coupling constants (J_a, J_a', and J_t); for the symmetric $Ni^{III}Ni^{II}Ni^{III}$ form there are only two (J_a, J_t), and for the last form only one (J_t) is required. All three models gave satisfactory fits (Table 5). The ground state of **14** is $S = 2$ irrespective of the model used, which is attained by ferromag-

Table 5. Magnetochemical Data of Complexes

	complex[a]	χ_{TIP}, 10^{-6} cm^3 mol^{-1}	μ_{eff}, μ_B	J_a,[b] cm^{-1}	J_t,[b] cm^{-1}	g	p.i.,[c] %	S_t[d]
1	$[L^0Ni^{II}Ni^{II}Ni^{II}L^0]$	100		+15	−6	2.0		3
2	$[LCo^{III}Co^{III}Co^{III}L]^{3+}$	1000					5 ($^3/_2$)	0
2*	$[LCo^{III}Co^{III}Co^{III}L]^{3+}$	460						0
3	$[LCo^{III}Ni^{II}Co^{III}L]^{2+}$	2600	2.95			2.1		1
4	$[LCo^{III}Ni^{III}Co^{III}L]^{3+}$	1390	1.82			2.1		$^1/_2$
5	$[LCo^{III}Ni^{IV}Co^{III}L]^{4+}$	840					3 (1)	0
6*	$[LNi^{II}Co^{III}Ni^{II}L]^+$	100			+7	2.2		2
7	$[LNi^{II}Co^{III}Ni^{III}L]^{2+}$	580			+20	2.3		$^3/_2$
8	$[LNi^{III}Co^{III}Ni^{III}L]^{3+}$	1740			+26	2.4	18 ($^3/_2$)	1
9*	$[LNi^{II}Ni^{II}Co^{III}L]^+$	1830		−61		2.2	3.2 (1)	0
10	$[LNi^{II}Ni^{III}Co^{III}L]^{2+}$	1920		+41		2.1		$^3/_2$
11	$[LNi^{III}Ni^{III}Co^{III}L]^{3+}$	1050		+81		2.2		1
12	$[LNi^{II}Ni^{II}Ni^{II}L]$	900		−28	+12	2.2		1
13*	$[LNi^{II}Ni^{III}Ni^{II}L]^+$	750		−20	+3	2.2		$^3/_2$
14	$[LNi^{III}Ni^{II}Ni^{III}L]^{2+}$	680		+44	−17	2.1		2
	$[LNi^{III}Ni^{III}Ni^{II}L]^{2+}$	770		+78/+46[e]	−2	2.1		2
	$[LNi^{II}Ni^{IV}Ni^{II}L]^{2+}$	270			+17	2.1		2
15	$[LNi^{III}Ni^{III}Ni^{III}L]^{3+}$	920		+93	+25	2.2		$^3/_2$
	$[LNi^{II}Ni^{IV}Ni^{III}L]^{3+}$	470			+52	2.2		$^3/_2$

[a] The formal oxidation states given are the basis for the fitting procedure, eq 1 (see text). [b] J_a represents the coupling constant between adjacent metal ions and J_t that between terminal metal ions. [c] Paramagnetic impurity with the assumed spin state in parentheses. [d] Ground state of the trinuclear species. [e] A modification of the HDvV model has been used with three different coupling constants J_a, J_a', and J_t (see text).

netic coupling between adjacent nickel ions in the first two models and by a ferromagnetic coupling between two terminal Ni^{II} ions in the last model.

The magnetic moment of **15** increases from 3.77 μ_B at 295 K to a plateau value of 4.28 μ_B at 10−30 K giving rise to an $S = {}^3/_2$ ground state. The X-band EPR spectrum of a solid sample of **15** is in agreement with this assignment: a rhombic signal with $g_x = 4.76$, $g_y = 3.37$, and $g_z = 2.00$ (Figure 10, bottom) is observed. Two oxidation state distribution models were used to fit the magnetic data of **15** to the HDvV model: $[LNi^{III}Ni^{III}Ni^{III}L]^{3+}$ and $[LNi^{II}Ni^{IV}Ni^{III}L]$. Both models gave an $S = {}^3/_2$ ground state and a satisfactory fit of the data.

Complex **1** has an $S = 3$ ground state which is attained by spin alignment of three octahedral Ni^{II} ions. An excellent fit of the data was obtained by using the HDvV formalism: a dominant ferromagnetic exchange coupling between adjacent nickel ions, $J_a = +15$ cm^{-1}, and a weak antiferromagnetic coupling between the terminal LNi^{II} moieties, $J_t = -6$ cm^{-1}, was calculated. Inclusion of a single-ion zero-field splitting parameter of $|D| = 11$ cm^{-1} improved the low-temperature fit significantly but it does by no means represent an accurate value. These values agree very nicely with those reported for $[Ni^{II}{}_3(acac)_6]$.[5]

The electronic spectra of complexes **2**−**15** have been measured in acetonitrile solution; they are displayed in the Supporting Information (Figures S1−S3). All complexes are highly colored and show intense ($\epsilon > 10^3$ L mol^{-1} cm^{-1}) absorption maxima in the visible (350−1200 nm). In general, in a given series of structurally similar complexes **3**−**5**, **6**−**8**, **9**−**11**, and **13**−**15** the number and intensity of these maxima increase with increasing oxidation levels. These transitions are predominantly thiolate-to-metal charge transfer and/or intervalence bands.

Discussion

By using the established rules for superexchange (Goodenough−Kanamori)[39] we first attempt to qualitatively rationalize the experimentally determined ground states of complexes **1**−**15**.

A superexchange mechanism to be operative in a polynuclear complex requires metal-centered localized oxidation states. In this sense the reported J values in Table 5 are parameters which describe magnetic exchange interactions in polynuclear compounds of class I according to the Robin and Day[40] classification.

In complexes **2**−**5** the terminal metal ions are always low-spin cobalt(III) ions. The LCo^{III} moiety is difficult to oxidize or reduce by one electron, respectively, which implies a localized oxidation state +III of the Co ion in all complexes containing the LCo^{III} moiety: **2**−**5** and **9**−**11**. On the other hand, the $[LNi^{II}]^-$ species containing an N_3S_3Ni octahedron is quite readily oxidized to $[LNi^{III}]$. Thus, in complexes containing one or two LNi fragments as in **9**−**11** and **6**−**8**, **12**−**15**, respectively, one cannot *a priori* assign a localized oxidation state to the nickel ion.

The central metal ion in the trinuclear complexes consists always of an MS_6 octahedral building block; it is NiS_6 in complexes **3**−**5**, **9**−**15**, and CoS_6 in complexes **2** and **6**−**8**. The electrochemistry of **2** and of analogous complexes from the literature demonstrates that the reduced form $Co^{II}S_6$ is accessible.[41] This is in agreement with the fact that the average Co−S distance in the reduced cobalt(II) form is very similar to that observed in the $Co^{III}S_6$ polyhedron (Table 4). Thus, if a cobalt ion is the central metal ion in the trinuclear complexes we cannot *a priori* discern between a +II or +III oxidation level of this ion. Since the inner-sphere Franck−Condon barrier to electron transfer $Co^{II}S_6 \rightleftharpoons Co^{III}S_6 + e^-$ is small,[42] the CoS_6 entity can facilitate electronic delocalization in the trinuclear species. Similarly, the octahedral NiS_6 core is known to readily accommodate the oxidation states II, III, and even IV at the central nickel ion.[37,38]

(39) (a) Goodenough, J. B. *Phys. Rev.* **1955**, *100*, 564. Goodenough, J. B. *J. Phys. Chem. Solids* **1958**, *6*, 287. (b) Kanamori, J. *J. Phys. Chem. Solids* **1959**, *10*, 87.

(40) Robin, M. B.; Day, P. *Adv. Inorg. Chem. Radiochem.* **1967**, *10*, 247.

(41) The one-electron reduced form of **2**, namely $[LCo^{III}Co^{II}Co^{III}L]^{2+}$, was generated electrochemically at −60 °C in acetone (0.10 M $[N(n\text{-}Bu)_4]PF_6$) and its X-band EPR spectrum has been recorded at 4.2 K. An $S = {}^3/_2$ signal (g values ∼4 and ∼2) with ^{59}Co hyperfine splitting was observed.

(42) (a) Küppers, H.-J.; Neves, A.; Pomp, C.; Ventur, D.; Wieghardt, K.; Nuber, B.; Weiss, J. *Inorg. Chem.* **1986**, *25*, 2400. (b) Küppers, H.-J.; Wieghardt, K.; Steenken, S.; Nuber, B.; Weiss, J. *Z. Anorg. Allg. Chem.* **1989**, *573*, 43.

If we follow the above arguments, it is evident that in complexes **3**, **4**, and **5** the central nickel ions have localized oxidation states of +II, +III, and +IV yielding the observed $S = 1$, $^1/_2$, and 0 ground states, respectively.

Complexes **9**, **10**, and **11** each contain only one terminal LCo^{III} unit and two adjacent nickel ions in an N_3S_3Ni and an NiS_6 environment. Since LCo^{III} has a localized low-spin cobalt(III) ion one can envisage these complexes as dinuclear exchange coupled nickel species. The synthetic route of **9** (Scheme 3, bottom) would imply that both nickel ions are in the oxidative state +II. The observed $S_t = 0$ ground state originates from an intramolecular antiferromagnetic coupling of two face sharing octahedral nickel(II) ions, which is mediated by three μ-thiophenolato bridges (see below).

One-electron oxidation of **9** yields the mixed valence species **10** which formally contains one terminal Ni^{II} and one central Ni^{III}. From the crystallographic results on **13*** and **14** we imply here that the central NiS_6 ion is a Ni^{III} ion and the terminal LNi unit contains Ni^{II}. The two nickel ions are again face sharing octahedral (in adjacent positions in the trinuclear dication). The experimentally determined $S_t = {}^3/_2$ ground state indicates a relatively strong *ferromagnetic* coupling in **10**. Thus, upon one-electron oxidation of **9** the sign of the coupling constant J_a changes from antiferromagnetic to ferromagnetic. In the frame of the Goodenough−Kanamori rules, interaction between a half-filled metal d orbital and an empty one results in spin alignment. In **10** a second interaction between two half-filled orbitals yields an antiferromagnetic contribution. The sum of both contributions determines the sign of the observed J value ($J = J_{AF} + J_F$) which is positive for **10**. In cases like this, the antiferromagnetic contribution is expected to be significantly larger than the ferromagnetic. Thus, the dominant ferromagnetic coupling in **10** is somewhat surprising.

Complex **11** contains the trication $[LNiNiCo^{III}L]^{3+}$ with an $S_t = 1$ ground state. Assuming a localized oxidation state distribution $[LNi^{III}Ni^{III}Co^{III}L]^{3+}$ in **11** the $S = 1$ ground state is attained by a ferromagnetic coupling between two adjacent low-spin Ni^{III} ions. On the other hand, if the central NiS_6 unit would contain a Ni^{IV} ion (low spin d^6) the terminal ion is Ni^{II} and a distribution $[LNi^{II}Ni^{IV}Co^{III}L]^{3+}$ would prevail, which could also be in agreement with the observed ground state. Obviously, it is difficult to satisfactorily rationalize these data in the localized oxidation state description.

Complexes **6***, **7**, and **8** contain two terminal LNi fragments and a central CoS_6 unit which is assumed to contain a low-spin Co^{III} ion. The two paramagnetic Ni ions are then separated by ~6 Å and the superexchange coupling is expected—and observed—to be weaker than in complexes where these ions are in adjacent positions (**9***, **10**, **11**). In complex **6*** containing an $[LNi^{II}Co^{III}Ni^{II}L]^+$ monocation an $S = 2$ ground state is attained via weak ferromagnetic exchange coupling. It is not possible to identify a convincing d orbital interaction pathway which orders the spins of the two localized Ni^{II} ions parallel. In the oxidized forms **7** with $[LNi^{II}Co^{III}Ni^{III}L]^{2+}$ and **8** with $[LNi^{III}Co^{III}Ni^{III}L]^{3+}$, again spin alignment yielding $S = {}^3/_2$ and 1 ground states, respectively, is observed.

Formally, the neutral species **12** contains three Ni^{II} ions, and a moderately strong antiferromagnetic coupling between adjacent nickel ions generates the observed $S_t = 1$ ground state. It is gratifying to note that the coupling in **12** and **9*** (with an $Ni^{II}Ni^{II}Co^{III}$ core) between adjacent nickel ions is antiferromagnetic in both cases, although this coupling is significantly stronger in **9*** than in **12**. The effective superexchange pathways are the same for both compounds (see below).

One-electron oxidation of **12** yields a mixed-valent monocation **13** for which—judging from the crystal structure determination—an oxidation state distribution of $Ni^{II}Ni^{III}Ni^{II}$ appears to be reasonable. Complex **13** has an $S_t = {}^3/_2$ ground state which is obtained by an antiferromagnetic coupling between the adjacent $Ni^{II}Ni^{III}$ ions and a very weak ferromagnetic coupling between the terminal LNi^{II} units. This behavior can be understood in the same fashion as described for **12** by using the Goodenough−Kanamori rules. Since the same two superexchange pathways between adjacent $Ni^{II}Ni^{III}$ ions in **13*** and **10** should be available, it is surprising that the sum of these contributions ($J = J_{AF} + J_F$) leads to a positive J_a value (ferromagnetic) in **10** but to a negative J_a in **13**. This is a further indication that the localized oxidation state description does not lead to a consistent picture of the observed ground states.

Complex **14** represents an interesting case; it has an $S = 2$ ground state. The following oxidation state distributions have been modeled: symmetric $[LNi^{III}Ni^{II}Ni^{III}L]^{2+}$ and asymmetric $[LNi^{III}Ni^{III}Ni^{II}L]^{2+}$. Although both gave reasonable fits (Table 5), these assignments are not in accord with the crystal structure of **14**. The dication is centrosymmetric which does not agree with the asymmetric form. Furthermore, upon one-electron oxidation of **13** (with a $Ni^{II}Ni^{III}Ni^{II}$ core) the Ni−S distances of the central NiS_6 unit in **14** *decrease* which rules out a central Ni^{II} ion but implies a central Ni^{IV} ion. This would give rise to a $[LNi^{II}Ni^{IV}Ni^{II}L]^{2+}$ distribution. It is possible to fit the magnetic data to this model. Note that for isoelectronic **6*** with a $Ni^{II}Co^{III}Ni^{II}$ core also a weak ferromagnetic coupling between two terminal Ni^{II} ions has been observed which is reasonable considering the fact that the two terminal paramagnetic centers are ~6 Å apart.

One-electron oxidation of **14** yields **15** for which a $[LNi^{III}Ni^{IV}Ni^{II}L]^{3+}$ oxidation state distribution is considered. The fit yields $J_t = +52$ cm^{-1} indicating a ferromagnetic coupling between two terminal ions, a Ni^{II} and a Ni^{III}, to give the observed $S = {}^3/_2$ ground state. On the other hand, it is also possible to obtain a good fit with the oxidation state distribution $Ni^{III}Ni^{III}Ni^{III}$. Then, the coupling between *adjacent* Ni^{III} ions is ferromagnetic as in complex **11**.

If the superexchange model is applicable for **1** and **12**, the following question arises: what are the relevant superexchange pathways in these structurally similar complexes or, more specifically, what is the difference between six phenolato bridging oxygen atoms in **1** and six thiophenolato bridging sulfur atoms in **12**? The Ni−O−Ni and corresponding Ni−S−Ni bond angles are different. The Ni−O−Ni angles are closer to 90° than the Ni−S−Ni angles which are more acute. The magnetic orbitals of the type $e_g||p_x\perp p_y||e_g$ are orthogonal at an Ni−X−Ni angle of ~90° and effect ferromagnetic coupling, whereas at angles <90° an antiferromagnetic exchange could become viable. In addition, the exchange pathway between half-filled e_g metal orbitals and the filled 3s orbital of the bridging sulfur, $e_g||s||e_g$, must be considered which yields an antiferromagnetic coupling. This pathway is not effective for the phenolato bridged complexes **1** and $Ni^{II}_3(acac)_6$ because the energies of the 2s oxygen and 3d metal orbitals are very different and, therefore, the overlap is small. Thus, the differing coupling between adjacent nickel ions in **1** and **12** can be understood by using the Goodenough−Kanamori rules.

To summarize the foregoing part of the discussion we conclude that the Goodenough−Kanamori rules for superexchange using localized metal oxidation states give a reasonably consistent picture of the coupling mechanism only for complexes

1 and **9*** and possibly for **12**, whereas they fail for complexes **6***, **7** and **8**, **10**, **11**, and **13***−**15**, which are, with the exception of **6***, **8**, and possibly **11**, mixed-valent species.

A major problem of the above superexchange analysis for **6**−**15** is the assumption of distinct localized oxidation states of the metal ions (class I complexes). That this is not the case—or at least an oversimplification—is at this point concluded primarily from (i) the results of the electrochemical investigation, (ii) the fact that the electronic spectra display more absorption maxima with increasing intensities in the NIR upon increasing the oxidation level of a given isostructural series of trinuclear complexes, and (iii) the general observation that bonds between a transition metal ion and RS^- bridges are more covalent than those of corresponding RO^- bridges facilitating thereby electron delocalization.

It is therefore likely that the present mixed valence complexes are class II or even III with substantial electron delocalization.

The interplay between electron exchange and electron transfer leads to the concept of double exchange[25e,f] which was first introduced by Zener in 1951 to account for parallel spin alignment in some mixed-valent $Mn^{III}Mn^{IV}$ perovskites,[24a] and was subsequently treated by Anderson and Hasegawa on a semiempirical level.[24b] In the spin-Hamiltonian approach of double exchange, an additional term which implies a resonance integral and a transfer operator is added to the usual HDvV superexchange term. Now the eigenenergies depend not only on the exchange coupling constant J but also on the transfer integral which increases with increasing covalent character of bonds of the bridging ligands.[43]

The archetype example for double exchange is $[Fe_2(\mu\text{-}OH)_3(tmtacn)_2]^{2+}$ where tmtacn represents 1,4,7-trimethyl-1,4,7-triazacyclononane. Mössbauer[27] and EXAFS spectroscopy[44] has shown that the excess electron is delocalized ($Fe_2^{2.5}$). An $S = {}^9/_2$ ground state is observed. This spin alignment is understood by a double exchange mechanism: two energetically equivalent resonance structures of the mixed-valent pair are mixed by a one-electron transfer as shown below.

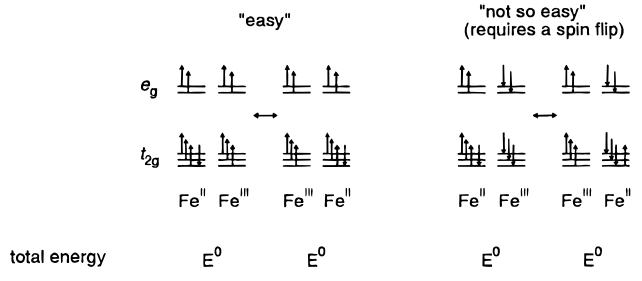

If the core spins of the two irons are aligned in a parallel fashion, the excess electron can be transformed from one side to the other without a spin flip. If the alignment of the core spins is antiparallel, the excess electron can only be transferred with a spin flip, otherwise a Pauli forbidden state would result. This transfer requires more energy. Therefore, the transfer of the excess electron leads to an effective ferromagnetic coupling of the two irons.

In this qualitative valence bond description the difference between a superexchange and the above double exchange mechanism results from the fact that superexchange is accomplished by electron transfer via an excited state which is mixed into the ground state by second-order perturbation, whereas double exchange occurs via ground state configurations only.[45] In this picture the total energy of the excited state is different from that of the both ground state configurations E^0 by the repulsion energy, U, of two electrons in one orbital:

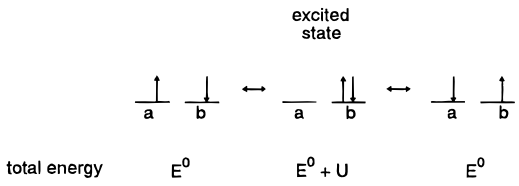

In accordance with our suggestion that electron delocalization plays an important role in the present system, we now attempt to qualitatively apply this simple concept to complexes **6**−**15**. For each complex it is possible to construct a number of resonance structures which are related by a one-electron transfer. In agreement with the concept of double exchange one-electron transfer generated resonance structures yielding Pauli forbidden states were excluded and, as a further constraint, one-electron transfer generated resonance structures must obey Hund's rule of maximal spin multiplicity at each metal center due to intraatomic exchange interaction. This is shown in Figure 12. Note that the constructed resonance structures are not necessarily energetically equivalent. The ground state of a given complex

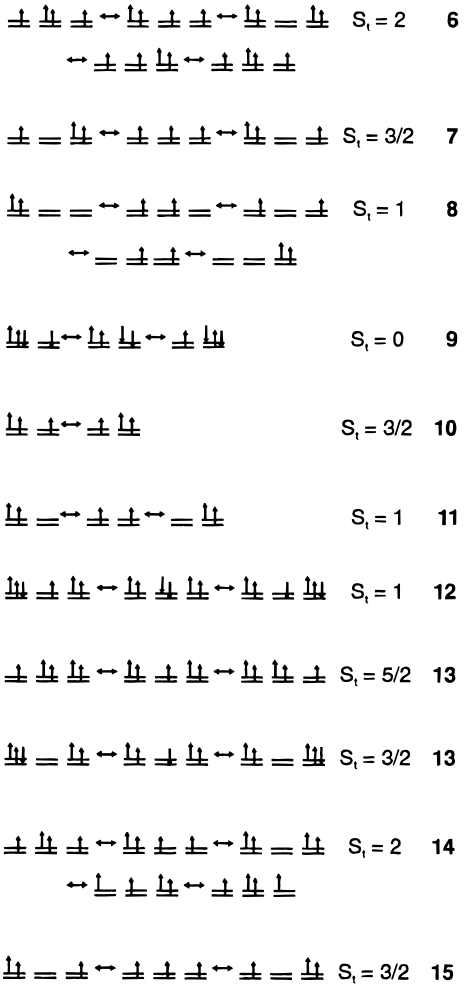

Figure 12. Resonance structures of complexes **6**−**15**. Only the degenerate e_g metal orbitals of the magnetically relevant metal ions in the trinuclear complexes are shown. For the sake of simplicity these orbitals were drawn at the same energy regardless of their differing donor sets (MS_6 or N_3MS_3).

(43) Kahn, O.; Girerd, J.-J. In *Studies in Inorganic Chemistry: Sulfur*; Müller, A., Krebs, B., Eds.; Elsevier: New York, 1984; Vol. 5, p 195.

(44) Peng, G.; van Elp, J.; Jang, H.; Que, L., Jr.; Armstrong, W. H.; Cramer, S. P. *J. Am. Chem. Soc.* **1995**, *117*, 2515.

(45) Kahn, O. In *Molecular Magnetism*; VCH Publishers: New York, 1993; (a) p 157, (b) p 337.

is then a linear combination of all resonance structures the individual weights of which may be different. Consequently, there always exists one resonance structure of lowest energy and largest weight to the ground state. For example, spin alignment in **6*** yielding $S_t = 2$ can readily be understood by applying these rules: the resonance structure $Ni^{II}Co^{III}Ni^{II}$ (Figure 12 middle structure) has the largest weight, whereas those for $Ni^{III}Co^{I}Ni^{III}$ (first and last structure in Figure 12) are minor contributors. The Co^{II} resonance structures in Figure 12 include low-spin Co^{II} appropriate to spin-allowed, single-electron transfer while for the known $Co^{III}Co^{II}Co^{III}$ species the EPR spectrum indicates $S = {}^3/_2$ (high-spin Co^{II}).

The above approach is somewhat intermediate between the classical double exchange mechanism with mixing of energetically equivalent resonance structures and a superexchange mechanism with mixing in of energetically highly excited states to the ground state.

In the following we discuss a few selected examples using the above delocalization model. Complex **13** represents an interesting case because the $Ni^{II}Ni^{III}Ni^{II}$ oxidation state distribution allows us to draw two different resonance structures, both of which are then related by one-electron-transfer steps to other resonance structures, respectively (Figure 12). Interestingly, this leads to different ground states, namely $S_t = {}^5/_2$ or ${}^3/_2$. Can one judge from the available data which is the more likely true ground state? The resonance structures associated with the ${}^5/_2$ ground state involve a central Ni^{II}, whereas for the ${}^3/_2$ ground state the central nickel ion has more Ni^{IV} character. From the crystallographic data of **13*** the latter appears to be the case and the $S = {}^3/_2$ ground state is the preferred one. Note that in this case the terminal nickel ions have some Ni^{I} character, whereas in **14** these ions have some Ni^{III} character. One would then predict that the Ni−S distances of the LNi fragments are shorter in **14** than in **13*** which is at least not contradicted by the data in Table 4. The difference in Ni−S bond lengths is −0.006 Å and not quite beyond the experimental error limit.

Another interesting case is complex **9** with two adjacent Ni^{II} ions. A resonance structure with parallel alignment of the four spins does not allow other one-electron-transfer structures to be drawn (Pauli); only an antiparallel arrangement allows the two other structures, shown in Figure 12, to be constructed. Delocalization thus enforces the observed $S_t = 0$ ground state.

It is very gratifying that within this delocalization model the electronic ground states of *all* complexes **6**−**15** are readily rationalized.

Conclusions and Summary

The hexadentate pendent arm macrocyclic ligands L^0H_3 and LH_3 provide a *cis*-tris(phenolate) or a *cis*-tris(thiophenolate) geometry in octahedral mononuclear L^0M^{III} or LM^{III} complexes, respectively. These complexes can function as ligands and form linear face-shearing homo- and heterotrinuclear complexes which contain six bridging phenolate or thiophenolate groups. Complexes of this type are ideally suited to study electronic coupling phenomena between three paramagnetic transition metal ions as a function of their respective d^n electron configuration. The following magnetostructural aspects have evolved from this study.

(1) The $S_t = 3$ ground state in $[Ni^{II}{}_3(acac)_6]$ and **1** is attained via a superexchange pathway where two adjacent Ni^{II} ions are ferromagnetically coupled ($e_g||p_x \perp p_y||e_g$) and a small antiferromagnetic coupling between the terminal Ni^{II} ions is characteristic for the Ni(μ-O)$_3$Ni(μ-O)$_3$Ni core.

(2) Replacement of the six phenolato bridges by thiophenolates as in **12** changes the sign of both J_a (now antiferromagnetic) and J_t (ferromagnetic). The $S_t = 1$ ground state of **12** is a consequence of the smaller Ni−S−Ni bridging angle as compared to the Ni−O−Ni angle, which cancels the orthogonality of the above magnetic orbitals and, in addition, a new antiferromagnetic pathway, $e_g||s||e_g$, is available because overlap between a filled 3s sulfur orbital and the half-filled e_g orbitals of nickel(II) is larger than between 2s oxygen orbitals.

(3) Trinuclear complexes containing two diamagnetic LCo^{III} moieties and a central nickel ion have localized oxidation states at the central metal ion: e.g. Ni^{II} in **3**, Ni^{III} in **4**, and Ni^{IV} in **5**.

(4) Two Ni^{II} ions in terminal positions as in **6** with a diamagnetic Co^{III} central ion order ferromagnetically ($S_t = 2$) whereas two Ni^{II} in adjacent positions as in **9** order antiferromagnetically. Only the latter effect is understood by using the Goodenough−Kanamori rules for superexchange. For the former, a delocalized model using the double exchange concept gives a straightforward explanation for the $S_t = 2$ ground state.

(5) Both mixed-valent complexes containing formally one Ni^{II} *and* an Ni^{III} ion either in adjacent *or* terminal positions relative to each other as in complexes **7** and **10** order strongly ferromagnetically ($S_t = {}^3/_2$). This is again most readily interpreted in terms of delocalization mechanisms. The delocalized excess electron aligns the spins. Similarly, the electron configuration of **10** and **13***, both containing adjacent $Ni^{II}Ni^{III}$ ions, cannot be understood in terms of superexchange mechanisms but the delocalization model proves to be useful.

(6) The ground states of $S_t = 2$ for **14** and $S_t = {}^3/_2$ for **15** can only be interpreted in terms of spin-dependent delocalization[45b] over all three nickel ions. This is, to the best of our knowledge, the first demonstration of this effect over *three* metal ions.

Acknowledgment. We thank Drs. J.-J. Girerd and G. Blondin (Paris-Orsay) for many hours of stimulating discussions on double exchange phenomena. Financial support of this work from the Fonds der Chemischen Industrie and the Deutsche Forschungsgemeinschaft (Schwerpunkt Bioanorganische Chemie) is gratefully acknowledged.

Supporting Information Available: Figures of the electronic spectra of complexes **2**−**11**, **13**−**15** in CH_3CN in the range 300−1200 nm; a table of elemental analyses data; tables of molar magnetic susceptibility data for complexes; tables of crystallographic data for **13*** and **14**; tables of positional and thermal parameters for all atoms, of interatomic distances and angles, and of anisotropic temperature factors (51 pages). See any current masthead page for ordering and Internet access instructions.

JA961305+